# Detecting Black Hole–Neutron Star Binaries with the Laser Interferometer Space Antenna

Thomas Wagg

A Thesis presented to the Department of Astronomy in partial fulfillment of the requirements for the degree of Bachelor of Arts

Contents

Acknowledgements

So, now I know how Frodo and Sam felt when they finally reached Mount Doom. Yet my journey along the way has been so much more enjoyable, mainly due to the help and support from all of the people below. Thank you to:

Floor, for being the best mentor that any student could hope for. Your constant help and advice has been invaluable throughout the process. You're always happy to explain things to me and meet at a moment's notice. You're not only a wonderful mentor but also a lovely person. Even when I struggled your encouragement made me feel as though I could do it.

Selma, for introducing me to an entirely new realm of astrophysics and infecting me with her enthusiasm. It was a good sign from the start when our 30 minute meeting somehow became two hours of me listening enraptured to you explaining different areas of your work. Even as a professor you are still able to make time to meet with me and answer my questions. Moreover, whether it is making sure that I'm not working at the weekend or helping me think through graduate school decisions, you make me feel valued not only as a researcher but also as a person.

Harshil, for his sage wisdom consistently imparted in the Mather Courtyard. You helped to start me on my path into research and I have learnt so much from you. Hopefully, in return, one day your path will lead to the 17th floor of the tower.

Nensi, for listening to me ramble about my thesis at all hours of the day. Your enthusiasm for my research was, well not entirely present, but you definitely listened and that's the main thing. Your love and humour are what keep me going when things get tough, I don't know what I'd do without you in my life.

Abstract

The detection of gravitational-waves emitted by double compact objects is starting to inform our understanding of the evolution of massive stars in binary systems. Black hole–neutron star (BH–NS) binaries are potentially observable with the planned space-based gravitational-wave detector LISA, which is sensitive to mHz frequencies. We estimate the number of BH–NS binaries that will be detected by LISA. Using BH–NSs generated from the rapid binary population synthesis code COMPAS, we calculate the signal-to-noise ratio for a each binary in LISA. Over the course of a 4-year LISA mission we estimate between 0 and 5 detections and we find the probability that there is at least one detection is 48%, assuming a signal-to-noise ratio threshold of 7. Extending the mission to 10 years improves this estimate to between 0 and 7 detections and a 69% probability. We demonstrate that, in principle, a BH–NS could be detected from galaxies as far as away as the Andromeda Galaxy. We show that these BH–NS binaries can typically be approximated as stationary gravitational-wave sources on the timescale of the LISA mission. We discuss the effect of different metallicity, eccentricity and star formation rate assumptions. Last, we discuss possible ways to distinguish BH–NS binaries from the far more numerous double white dwarf background. We conclude that BH–NS binaries will be an exciting class of sources potentially detectable by the future LISA mission that will help in refining models of massive binary evolution.

Glossary

Here we provide an overview of the terms and acronyms used throughout this thesis and also in common use in the literature.

BH *Black Hole*   A singularity in space that is so dense that no light can escape its event horizon

BHNS *Black Hole Neutron Star* A binary system composed of one black hole and one neutron star

CBB *Case BB Mass Transfer* Stable mass transfer from secondary to primary star with Hertzsprung gap star as donor

CE   *Common Envelope* A state in binary evolution in which both stars in a binary system are contained in a common envelope of gas

CO   *Compact Object*   A compact remnant of a star, either a white dwarf, a neutron star or a black hole

DCO *Double Compact Object* A binary system of two compact objects

GW *Gravitational Waves* Disturbances in the curvature of spacetime, generated by accelerated masses that propagate at the speed of light

IMF	*Initial Mass Function*	A function describing the initial distribution of the masses of stars in a population
KDE	*Kernel Density Esimtator*	A statistical tool for estimating the probability density function of a random variable
LIGO	*Laser Interferometer Gravitational-Wave Observatory*	A ground-based Gravitational-Wave detector, sensitive to kHz frequencies
LISA	*Laser Interferometer Space Antenna*	A planned space based Gravitational-Wave detector, sensitive to mHz frequencies
MS	*Main Sequence*	The phase of stellar evolution where stars are burning hydrogen in their centre
NS	*Neutron Star*	A stellar remnant of extreme density and small radius, composed almost entirely of densely packed neutrons
RL	*Roche Lobe*	The volume around a star, within which material is gravitationally bound to the star
SN	*Supernova*	A stellar explosion at the end of a massive star's life, typically leaves behind a neutron star or black hole
SNR	*Signal-to-Noise Ratio*	The ratio between the signal and the background noise, used for assessing detectability
ZAMS	*Zero-Age Main Sequence*	A classification for stars that have just started central hydrogen burning

Chapter 1

Introduction

In 2015, the LIGO and Virgo collaborations opened a new realm of astrophysics with the first direct detection of gravitational waves (Abbott et al., 2016). They detected the waves emitted by a merger of two black holes, thereby confirming the existence of stellar-mass binary black hole systems. The discovery spurred a new movement to use gravitational waves to explore a new view of the Universe.

Gravitational waves are an analogue of the light emitted when accelerating charged particles. Particular configurations of accelerated masses radiate energy in the form of gravitational waves. Gravitational waves differ from electromagnetic waves in ways that make them extremely interesting for astrophysics.

Firstly, gravitational-wave detectors measure the amplitude of the waves whereas conventional telescopes measure the intensity of light. This is a critical difference, since the amplitude of a gravitational wave scales as $1/d$ whereas intensity scales as $1/d^2$ and so this favours the detection of sources at larger distances. Moreover, in principle we can detect gravitational waves from parts of the universe that electromagnetic radiation cannot bypass. For example, before the universe reached the stage of recombination, it was opaque to light. This is because, before recombination, free electrons would scatter photons in random directions and this prevents the light from reaching us. Yet, gravitational waves have no such limits and so we could learn more about double compact object at high redshift and the early universe with future generations of detectors.

One proposed source of gravitational waves is a black hole–neutron star binary (BH–NS). This is a bound system with one black hole and one neutron star, which sprial inwards, eventually resulting in a merger. At the time of writing, no unambiguous detection of a BH–NS system has been reported, although there have been several candidates. Yet, detecting one of these fascinating binary systems will have many exciting implications.

Current theories on the formation of these binaries are extremely uncertain, with predictions for formation rates ranging across four orders of magnitude. Therefore, the number of detections in LISA will be critical in informing which theories have made the most accurate predictions. This will help us to refine our understanding of the remnants and evolution of massive stars. Moreover, collating a sample of BH–NS binaries will allow us to better understand whether there are electromagnetic counterparts to their gravitational wave signal, especially during their merger. This could come in the form of gamma-ray bursts, pulsars or even kilonovae.

A sample of BH–NS binaries would also allows us to better understand which types of black holes are paired with which types of neutron stars. It is currently unclear whether certain mass ratios or other relationships are more favourable for a stable BH–NS binary. Identifying these relationships could help us to better understand BH–NS formation. Finally, if the neutron star is observable (for example as a pulsar), a BH–NS would be ideal for measuring the Hubble constant, testing general relativity and learning more about black holes. It is extremely difficult to measure the parameters of a black hole directly and so we rely on indirect means. Therefore, if we can observe the neutron star in a BH–NS, it is possible to infer the properties of the black hole from measuring its effect on the neutron star.

Although we are not sure how these binaries are formed, a standard formation channel has been commonly considered (e.g. Flannery & van den Heuvel, 1975; Smarr & Blandford, 1976; Srinivasan, 1989; Tauris & van den Heuvel, 2006; Belczynski et al., 2008; Kruckow, Tauris, Langer, Kramer, & Izzard, 2018) and we shall describe this here. The formation is also shown in Fig. 1.1.
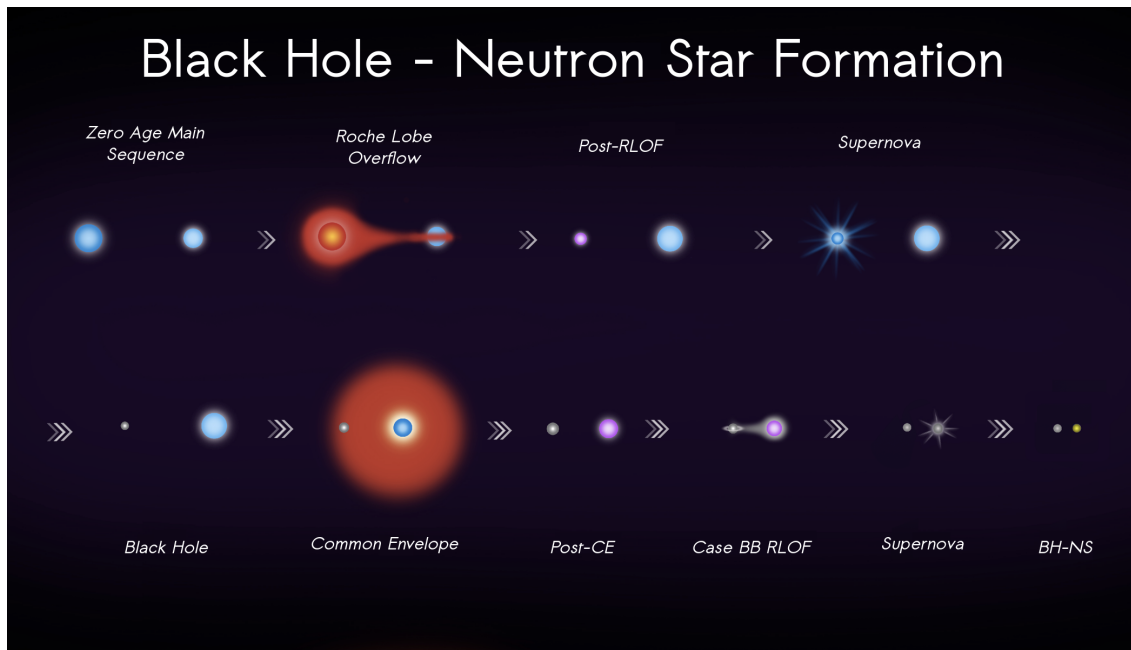
Figure 1.1: A diagram of the standard formation channel of a black hole neutron star binary system. This figure is based on Fig 1. from Vigna-Gómez et al. (2020) by T. Rebagliato which is publicly available.

The BH–NS starts as a binary system of two massive stars orbiting one another in isolation. As the stars evolve, one (the primary star) will expand beyond its Roche lobe, such that the material is no longer gravitationally bound to the star. At this point the pimary star will initiate mass transfer onto its companion. The primary star typically transfers its entire hydrogen envelope and eventually goes supernova, leaving behind either a black hole or a neutron star depending typically on the mass of the star. Let us assume the primary star becomes a black hole in this case as this is the most common formation path in simulations that we use.

After the supernova, the secondary star expands in a similar manner and exceeds its own Roche lobe. But now the mass transfer is unstable, initiating a common envelope (CE) phase, in which the compact remnant of the primary star and the core of the secondary star are contained within a shared gas envelope that is formed from the donor's envelope. The gas results in drag and torque forces on the two cores, causing them to lose angular momentum and significantly decrease their separation. If the envelope is ejected successfully, it leaves behind the black hole and a helium star. Otherwise, the black hole and core of the secondary star merge without ejecting

the envelope and so never form a BH–NS. In a subset of the binaries there is a stable case BB mass transfer phase after the CE from the helium star onto the primary compact object. This typically occurs when the secondary is a relatively low mass helium star. The helium star eventually goes supernova and leaves behind a neutron star. If the system remains bound, the resulting system is now a black hole–neutron star binary in a short orbit. It is important to note that each of these phases could be unsuccessful and prevent the formation of a binary. The probability of success at each stage is considered in section 2.1.4.

A planned gravitational wave detector that could observe these BH–NS systems is the Laser Interferometer Space Antenna (LISA) (Danzmann & Rüdiger, 2003). It will be formed of three satellites separated by 5 million kilometres, which relay laser beams in an equilateral triangle. As a gravitational wave passes through the instrument, the laser will take slightly more or less time to reach the next satellite. Based on the change in the time that the laser is received, one can calculate the strain, or change in length per unit length, exerted by the gravitiational waves.

Figure 1.2: An artist's impression of the LISA detector in operation. Three satellites, separated by millions of kilometres and precisely relaying lasers in orbit behind the Earth. This image is taken from LISA mission multimedia gallery.
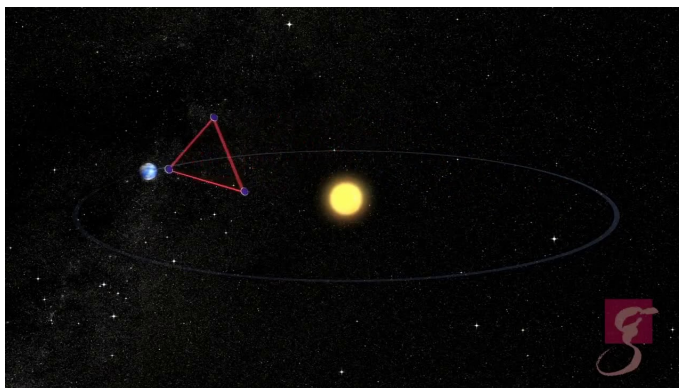
LISA is also by no means simply 'LIGO in Space'. LIGO is sensitive to frequencies approximately between 10–1000 Hz, allowing it to observe the mergers of stellar-mass binary systems. However, LISA's sensitivity will range from approximately 10^{-4}–10^{-1} Hz and so it will be able to detect stellar mass systems before they merge. The benefit of seeing these wider binaries is that they will be approximately stationary in their inspiral, meaning that the separation of the two stars will remain near constant for the duration of the mission.

As mentioned above, we have not yet successfully detected a BH–NS system and so it is important to know how many of these systems we expect LISA to detect and what we can learn about them using this detector. In this thesis, we calculate a detection rate for a four-year LISA mission by simulating the population of tens of thousands of BH–NS systems within the Milky Way and analysing which would be detectable at the time of the LISA mission.

In chapter 2, we perform some back-of-the-envelope estimations that have guided us during this project. We have included them here as they provide insight into the problem and an upper bound on the number of detections we could expect during LISA. In chapter 3, we explain our methods of simulating the BH–NS systems, both in their formation and evolution in the Milky Way and how we determine whether a system is detectable by LISA. In chapters 4 and 5, we present the results of our simulation and discuss the implications for the LISA mission.

Chapter 2

A Survey of the Problem Based on Analytical Estimations

In order to estimate the feasibility of the project and provide insight into the problem, we begin by performing a series of back-of-the-envelope estimations of an upper bound on the rate of BH–NS systems that can be observed with LISA. The goal is to provide a rough assessment whether LISA is likely to detect *any* black hole neutron star (BH–NS) binary system within its lifetime. We only consider galactic BH–NS systems in these estimations, since any systems from outside the Milky Way are much harder to detect and so not expected to contribute as significantly. However, we will show that, in principle, we can detect BH–NS systems as far out as the Andromeda Galaxy.

We frame these estimations with three questions and explore each in detail in the following sections.

- How many BH–NS systems do we expect to exist in our galaxy? (Section 2.1)

- Out to what distance are these systems detectable with LISA? (Section 2.2)

- How long could we observe each system within the LISA band? (Section 2.3)

2.1 Total BH–NS systems in the Milky Way

In this section we estimate the total number of BH–NS binaries in the Milky Way. We start by finding the fraction of stars that have ended their lives as black holes today, based on the formation history of the Milky Way, which is discussed in sections 2.1.1 and 2.1.2. We convert this fraction to a total *number* of black holes in the galaxy by using the total mass of the galaxy and the expected mass, as shown in section 2.1.3. Finally, in section 2.1.4, we make a rough estimate of the fraction of black holes that form a BH–NS system and use this fraction to find the overall total number of BH–NS systems in the Milky Way.

2.1.1 Initial Distribution of Stars

The Initial Mass Function (IMF) describes the initial distribution of masses of stars, i.e. the number for stars $\mathrm{d}N$ with masses between m and $m+\mathrm{d}m$. We use the broken power law from Kroupa (2001), an IMF given by

$$\zeta(m) = \beta(m) \cdot m^{-\alpha(m)}, \tag{2.1}$$

where m is the mass of the star and $\alpha(m)$ is defined as

$$\alpha(m) = \begin{cases} 0.3 \pm 0.7 & 0.01 \leq m < 0.08, \\ 1.8 \pm 0.5 & 0.08 \leq m < 0.50, \\ 2.7 \pm 0.3 & 0.50 \leq m < 1.00, \\ 2.3 \pm 0.7 & 1.00 \leq m, \end{cases} \tag{2.2}$$

and $\beta(m)$ are normalisation coefficients. In order to calculate $\beta(m)$ we enforce that the function is continuous and is normalised for our defined mass range. For the purpose of these estimations we define this range as $0.01\,\mathrm{M_\odot} \leq m \leq 150\,\mathrm{M_\odot}$ (Figer, 2005; Kasper et al., 2007). The values of β are given by

$$\beta(m) = \begin{cases} 2.66 & 0.01 \le m < 0.08, \\[2mm] 0.06 & 0.08 \le m < 0.50, \\[2mm] 0.03 & 0.50 \le m < 1.00, \\[2mm] 0.03 & 1.00 \le m. \end{cases} \tag{2.3}$$

By ensuring the integral is normalised, $\zeta(m)$ is a probability density function. Henceforth in these estimations we will neglect the uncertainties on the values of α.
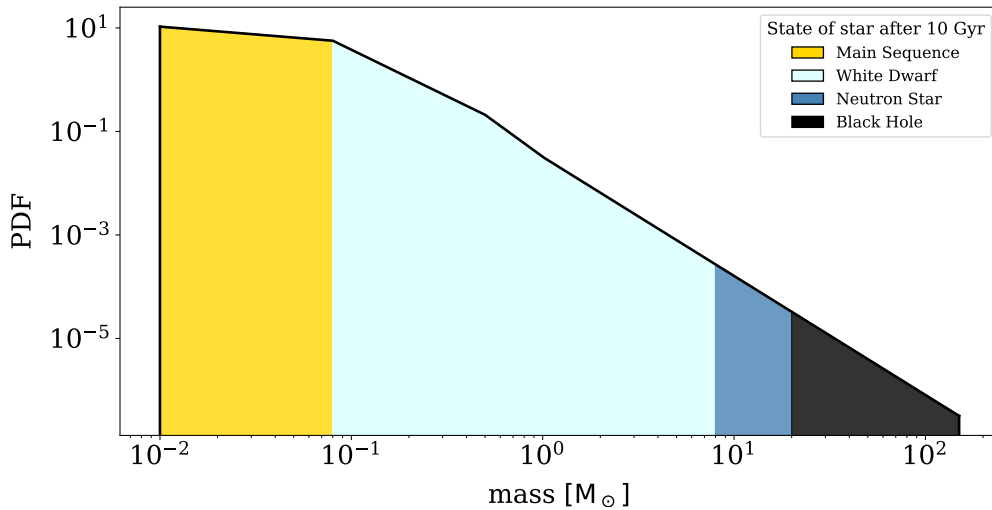
Figure 2.1: The initial mass function from Kroupa (2001). The colours indicate the assumed final fate of a single star produced from each mass range after 10 Gyr.

For these estimations, we make the assumption that stars in particular mass ranges have a similar final fate. Thus we assume that stars with initial mass between 0.08 and $8\,M_\odot$ become white dwarfs, between 8 and $20\,M_\odot$ become neutron stars and between 20 and $150\,M_\odot$ become black holes. Stars with masses less than $0.08\,M_\odot$ do not evolve off the main sequence within the timescale of 10 Gyr, the age of the Milky Way (see however Heger, Fryer, Woosley, Langer, & Hartmann, 2003, for a more sophisticated picture). It is important to note that this is a simplifying assumption. In reality, it is unlikely that massive star evolution has sharp boundaries at discrete mass values. A more realistic view is that the final fate is probabilistic and depends on a variety of factors, not just the mass (e.g. Sukhbold, Ertl, Woosley, Brown,

& Janka, 2016, Fig. 13). This would affect our rate of detection for BH–NS, yet the uncertainty on this is outweighed by the uncertainty on particular phases of massive stellar evolution (such as the common envelope phase). Therefore, it is likely a reasonable assumption to have clear boundaries for the purpose of these rough estimates.

2.1.2   Fraction of Stars that are Black Holes

The fraction of stars in the Milky Way that have formed black holes today is dependent on the assumed star formation history. If a star was only born very recently, it will not have had time to evolve into a black hole and this will affect the fraction. This formation history of the galaxy can be approximated in several ways, but for this estimate we only consider two simplified formation histories: a starburst and continuous Star formation. These simplifications assume, respectively, that all stars were created at the start of the galaxy and that the galaxy creates stars at a uniform rate throughout the galaxy's lifetime. We now consider how these approximations, in conjunction with the initial mass function, will affect the fraction of stars that are black holes in our galaxy today.

Starburst Formation

As a simple starting point, we assume that all stars are formed during a starburst at the start of the galaxy's life and that there has been no star formation since then. This is not a realistic assumption, but the simplest one to compute, so will consider this first. If we take the age of the galaxy to be 10 Gyr, this means that every star that was destined to die and become a black hole will have been alive long enough to do so, since the lifetime of stars forming black holes is much smaller than 10 Gyr.

In the starburst formation galaxy, the fraction of stars that were destined to become black holes at the inception of the galaxy is therefore equal to the fraction of stars that are currently black holes. This simplification allows us to simply integrate the IMF between the mass range of black hole progenitors in order to find this

fraction

$$f_{\mathrm{BH,burst}} = \int_{20\,\mathrm{M_\odot}}^{150\,\mathrm{M_\odot}} \zeta(m)\,\mathrm{d}m \approx 5 \times 10^{-4}. \tag{2.4}$$

Continuous Star Formation

Alternatively, a less drastic assumption is that the galaxy has been continuously forming stars since its inception. This is a more realistic assumption, see for example Mor, Robin, Figueras, Roca-Fàbrega, and Luri (2019). The key difference here is that not all stars will have had enough time to die by today. For simplicity, we assume that the evolution times are: $5\,\mathrm{Gyr}$ for white dwarf progenitors, $50\,\mathrm{Myr}$ for neutron star progenitors and $5\,\mathrm{Myr}$ for black hole progenitors.

Using these assumptions, we find that using constant star formation for black holes, the fraction of stars that have formed a black hole is $1 - 5\,\mathrm{Myr}/10\,\mathrm{Gyr} = 0.9995$. So we find roughly the same fraction for black holes as for a starburst formation history

$$f_{\mathrm{BH,cont.}} = 0.9995 \cdot f_{\mathrm{BH,burst}}. \tag{2.5}$$

Note that only half of white dwarf progenitors will have had enough time to evolve to a white dwarf over the lifetime of our galaxy. Therefore, we would have had drastically different results if we were interested in white dwarfs.

2.1.3   Total number of Black Holes

The fraction of stars that are black holes can be converted to a total number of black holes by using the mass of the Milky Way to find the total number of stars. Licquia and Newman (2015) found that the total mass formed in stars in the Milky Way is approximately $M_{\mathrm{MW}} \approx 10^{11}\,\mathrm{M_\odot}$. Therefore, the total number of stars in the galaxy, N_{MW}, is approximately the total mass of the galaxy divided by the average stellar mass

$$N_{\mathrm{MW}} \approx \frac{M_{\mathrm{MW}}}{\langle m \rangle} \approx 4.7 \times 10^{11}, \tag{2.6}$$

where we approximate

$$\langle m \rangle = \int_{0.01\,\mathrm{M}_\odot}^{150\,\mathrm{M}_\odot} \zeta(m) \cdot m \, \mathrm{d}m \approx 0.21. \qquad (2.7)$$

Multiplying the black hole fraction with N_{MW} gives that the total number of black holes in the galaxy is

$$N_{\mathrm{BH}} = f_{\mathrm{BH,cont.}} \cdot N_{\mathrm{MW}} \approx 2.2 \times 10^8, \qquad (2.8)$$

or about two hundred million.

2.1.4 Fraction of Black Holes in BH–NS Systems

Not all black holes are part of a BH–NS system and so we need to calculate the subpopulation of these systems to get the correct number of BH–NS in the Milky Way. Although a large fraction of massive stars are born in binaries (Sana et al., 2012), the majority of these systems disrupt during different stages of their formation. Therefore, in order to calculate how many black holes become part of a BH–NS system, the fractions of binaries that survive each stage of the system formation has to be considered. For a typical formation history of a double compact object see Fig. 1.1. The total fraction of black holes that are in BH–NS systems can then be written as a multiplication of fractions that survive each stage of evolution

$$f_{\mathrm{BHNS}} = f_{\mathrm{bin}} \cdot f_{\mathrm{q}} \cdot f_{\mathrm{SN1}} \cdot f_{\mathrm{CE}} \cdot f_{\mathrm{SN2}} \cdot f_{\mathrm{Hubble}}. \qquad (2.9)$$

In the rest of this section we explain in detail the definition and typical values that we have assigned each of these fractions.

f_{bin}**: What fraction of black hole progenitors form in binaries?**

Recent studies have shown that most massive stars are formed in binaries (e.g. Sana et al., 2012). Only 29% of massive stars are effectively single (Sana et al.,

2012). Using this, the fraction of black hole progenitors that form in binaries is then typically

$$f_{\rm bin} \approx 0.7. \tag{2.10}$$

$f_{\rm q}$: Does the system have the required mass ratio?

In order for the companion star to become a neutron star, it must be sufficiently massive. Moreover, if one star is significantly less massive than the other star, the system typically leads to a stellar merger, leaving behind a single star. Therefore, this restricts the mass ratio from being excessively low for binaries forming a BH–NS. We assume the mass ratio, $q = m_2/m_1$ must be at least 0.25 (e.g. Wellstein, Langer, & Braun, 2001). If we assume that the birth mass ratio distribution is roughly uniform (e.g. Moe & Di Stefano, 2017), this removes a quarter of systems,

$$f_{\rm q} \approx 0.75. \tag{2.11}$$

$f_{\rm SN1}$: Does the system remain bound after the first supernova?

There is typically a drastic mass loss during the first supernova leading to the binary system becoming unbound. This affects a significantly large fraction of candidate systems (e.g. Renzo et al., 2019), giving a typical survival fraction of

$$f_{\rm SN1} \approx 0.1. \tag{2.12}$$

$f_{\rm CE}$: Does the system survive common envelope phase?

Additionally, these systems typically undergo a common envelope event. However, only a small fraction of systems both have secondary stars that expand enough for a Roche-lobe overflow that leads to the common envelope, and successfully eject their envelope without a stellar merger (e.g. Vigna-Gómez et al., 2018a), giving a typical survival fraction of

$$f_{\rm CE} \approx 0.25. \tag{2.13}$$

f_{SN2}: **Does the system remain bound after the second supernova?**

In order to successfully form a BH–NS, the binary also needs to stay bound after the second supernova. Although it is still uncertain, more systems typically remain bound after the second supernova than after the first (e.g. Vigna-Gómez et al., 2018a). This is mainly due to the fact that the binary becomes more tightly bound after the common envelope phase. From Vigna-Gomez we obtain a typical value of

$$f_{\mathrm{SN2}} \approx 0.4. \tag{2.14}$$

f_{Hubble}: **Is the system compact enough to merge in a Hubble time?**

Finally, it is important that we confirm that the system will eventually merge and pass through the LISA band. This is approximately the fraction of systems that merge in a Hubble time, which we can calculate using the work of Peters, 1964 (as will be discussed in 2.3). This assumption rules out roughly half of the binaries (e.g. Vigna-Gómez et al., 2018a), giving

$$f_{\mathrm{Hubble}} \approx 0.5. \tag{2.15}$$

The binary has to survive all these phases and so we apply each of these fractions together to find an estimate for the fraction of black holes that exist in BH–NS systems

$$f_{\mathrm{BHNS}} = 2.6 \times 10^{-3} \left(\frac{f_{\mathrm{bin}}}{0.7} \right) \left(\frac{f_{\mathrm{q}}}{0.75} \right) \left(\frac{f_{\mathrm{SN1}}}{0.1} \right) \left(\frac{f_{\mathrm{CE}}}{0.25} \right) \left(\frac{f_{\mathrm{SN2}}}{0.4} \right) \left(\frac{f_{\mathrm{Hubble}}}{0.5} \right). \tag{2.16}$$

Applying this fraction to the number of black holes, we find that the total number of BH–NS systems that we estimate to exist in the milky way and merge in a Hubble time is

$$N_{\mathrm{BHNS}} = f_{\mathrm{BHNS}} \cdot N_{\mathrm{BH}} \approx 5.7 \times 10^5, \tag{2.17}$$

or roughly half a million.

2.2 Maximum Detectable Distance with LISA

As mentioned in the introduction, the LISA detector measures the strain, which is the change in length of the detector per unit length, caused by gravitational waves. This strain, assuming that the binary is circular and stationary in frequency space, is given by

$$h = \sqrt{\frac{64}{5}} \frac{(G\mathcal{M}_c)^{5/3}(\pi f)^{2/3}}{Dc^4}, \tag{2.18}$$

where D is the distance to the binary, f is the gravitational wave frequency and $\mathcal{M}_c$ is the chirp mass, defined as

$$\mathcal{M}_c = \frac{(m_1 m_2)^{\frac{3}{5}}}{(m_1 + m_2)^{\frac{1}{5}}}. \tag{2.19}$$

Conveniently, this strain only falls off as $1/D$ with increasing distances, a stark contrast to the $1/D^2$ for electromagnetic radiation. However, a more useful parameter is the *characteristic* strain. This is given by (e.g. Finn & Thorne, 2000)

$$h_c = h\sqrt{\frac{2f^2}{\dot{f}}}, \tag{2.20}$$

where $\dot{f}$ is given by

$$\dot{f} = \frac{96}{5\pi} \frac{(G\mathcal{M}_c)^{5/3}(\pi f)^{11/3}}{c^5}, \tag{2.21}$$

and so the explicit definition of the characteristic strain is

$$h_c = \sqrt{\frac{2}{3}} \frac{(G\mathcal{M}_c)^{5/6}}{Dc^{3/2}} \frac{1}{(\pi^4 f)^{1/6}} \tag{2.22}$$

The characteristic strain is more useful as it more accurately represents the signal strength used in calculating the signal-to-noise ratio. This is because, as the BH–NS spirals inwards, the signal detected from LISA is not just from a single cycle. Since BH–NS systems in the LISA band move very slowly through frequency space (see section 2.3), a BH–NS will emit the same frequency gravitational waves for a significant period of time, over many cycles. Therefore, the detector can measure

every cycle and so enhance the signal in comparison to the detector noise. A BH–NS spends $f^2/\dot{f}$ cycles in the vicinity of the frequency f. Hence, the signal strength is approximately the same as a signal with strain $h_c = h\sqrt{2f^2/\dot{f}}$.

If we take a typical BH–NS with a black hole of mass $10\,\mathrm{M_\odot}$ and a neutron star of mass $1.4\,\mathrm{M_\odot}$, we find a typical BH–NS chirp mass of approximately $3\,\mathrm{M_\odot}$. Since most stars are found at the centre of the Milky Way (e.g. McMillan, 2011), we can use a typical distance of $8\,\mathrm{kpc}$, as this is the distance from the Earth to the centre of the Milky Way. The gravitational wave frequency to which LISA is most sensitive (see next section 2.2.1) is roughly $4 \times 10^{-3}\,\mathrm{Hz}$. Plugging in these parameters we find the following scaling relations for the strains.

$$
\begin{aligned}
h &= 2.1 \times 10^{-21} \left(\frac{\mathcal{M}_c}{3\,\mathrm{M_\odot}} \right)^{\frac{5}{3}} \left(\frac{D}{8\,\mathrm{kpc}} \right)^{-1} \left(\frac{f}{4 \times 10^{-3}\,\mathrm{Hz}} \right)^{\frac{2}{3}}, \\
h_c &= 1.1 \times 10^{-16} \left(\frac{\mathcal{M}_c}{3\,\mathrm{M_\odot}} \right)^{\frac{5}{6}} \left(\frac{D}{8\,\mathrm{kpc}} \right)^{-1} \left(\frac{f}{4 \times 10^{-3}\,\mathrm{Hz}} \right)^{-\frac{1}{6}}.
\end{aligned}
\tag{2.23}
$$

The magnitude of the characteristic strain compared to the LISA sensitivity curve determines whether LISA can detect the binary system.

2.2.1 LISA Sensitivity Curve

The LISA sensitivity curve, $S_n(f)$, shown in Fig. 2.2, is used for assessing what signals are detectable (Robson, Cornish, & Liu, 2019). Any characteristic strain below the curve cannot be distinguished from noise, but sources causing strains above the sensitivity curve may possibly be detected. For sources above we can calculate the sky-averaged signal-to-noise ratio and use this to estimate which sources are detectable. This is calculated in Section 2.2.2.

In addition to the curve, Fig. 2.2 shows the strain for BH–NS systems at different distances. These systems each have $m_{\mathrm{BH}} = 10\,\mathrm{M_\odot}$ and $m_{\mathrm{NS}} = 1.4\,\mathrm{M_\odot}$, giving the typical chirp mass of $\mathcal{M}_c \approx 3\,\mathrm{M_\odot}$. Moreover, each system is assumed to have the optimal frequency, $f \approx 4 \times 10^{-3}\,\mathrm{Hz}$, that is at the minimum of the LISA sensitivity curve. This figure shows not only that systems in the Milky Way are detectable,
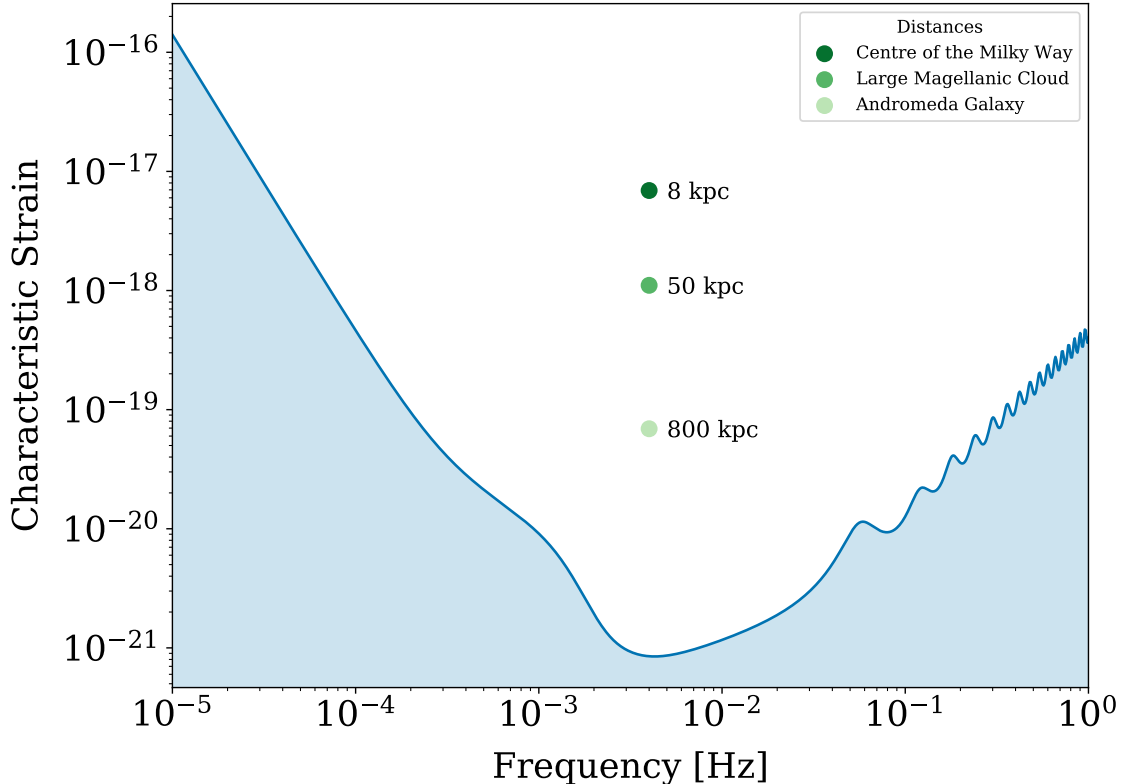
Figure 2.2: The characteristic strain that would be measured for a BH–NS system emitting the gravitational waves at the optimal frequency of $f \approx 4 \times 10^{-3}$ Hz and with masses $10 \, M_\odot$ and $1.4 \, M_\odot$ at different distances. The blue line is the LISA sensitivity curve, plotted using Robson, Cornish, and Liu (2019), below which systems are undetectable. This illustrates that we could not only theoretically detect all BH–NS systems in the Milky Way that emit at this frequency but also that detections of BH–NS systems up to the Andromeda Galaxy are possible.

but also that BH–NS detections as far as the Andromeda Galaxy at 800 kpc are possible. Unfortunately, as we will show in the next chapter of this thesis, DCO's with the optimal frequency are extremely rare.

2.2.2   Signal-to-Noise Ratio

A key estimator for the detectability of a source is the signal-to-noise ratio (SNR). Following Breivik et al. (2019), if we average the strain across sky location, inclination and polarisation, the most general equation for calculating the SNR of a binary system that is both eccentric and moving in frequency space is

$$(\text{SNR})^2 = \sum_{n=1}^{\infty} \int_{f_{\text{start}}}^{f_{\text{end}}} \left[\frac{h_{c,n}\left(f_n\right)}{h_f\left(f_n\right)} \right]^2 \mathrm{d} \ln f_n, \tag{2.24}$$

where we integrate over the frequency space that the binary traverses and sum over the different harmonics of gravitational waves that the eccentric binary emits. However, for binaries that are circular and stationary in frequency space on the timescale of the LISA mission, the frequency does not vary significantly and all gravitational wave power is emitted in the $n = 2$ harmonic. We can therefore neglect the integral and sum, reducing the equation to

$$\mathrm{SNR} = \frac{h(f)}{\sqrt{S_n(f)}} \cdot \sqrt{T_{\mathrm{obs}}}, \tag{2.25}$$

where T_{obs} is the LISA mission duration in seconds and $S_n(f)$ is the LISA sensitivity curve. Henceforth, we consider a signal-to-noise ratio of 7 to be the threshold for detections in LISA. Earlier papers demonstrated that the threshold for detection should be 5 (Crowder & Cornish, 2007) or 5.7 (Błaut, Babak, & Królak, 2010). However, these investigations did not consider the second derivative of the frequency or the orbital eccentricity, which could be useful for identifying systems undergoing mass transfer or triple systems (e.g. Nelemans, Yungelson, & Portegies Zwart, 2004; Robson, Cornish, Tamanini, & Toonen, 2018; Tamanini & Danielski, 2019; Korol et al., 2020). Therefore, similar to Korol et al, we adopt this conservative threshold of 7.

The detectability of BH–NS systems depends on their mass, distance and frequency. We consider neutron star masses between 1 and $3\,\mathrm{M}_\odot$ and black hole masses between 5 and $35\,\mathrm{M}_\odot$ (e.g. Farr et al., 2011). This gives a chirp mass range of approximately 2 to $8\,\mathrm{M}_\odot$. In Fig. 2.3, we plot the signal-to-noise ratio for systems with these masses at distances up to $10\,\mathrm{Mpc}$, for BH-NS systems at a fixed optimal frequency of $f \approx 4 \times 10^{-3}\,\mathrm{Hz}$, which therefore is an upper bound on the signal-to-noise ratio for systems of these masses and distances.

Fig. 2.3 shows that it, in principle, possible to detect systems as far as the Andromeda galaxy.
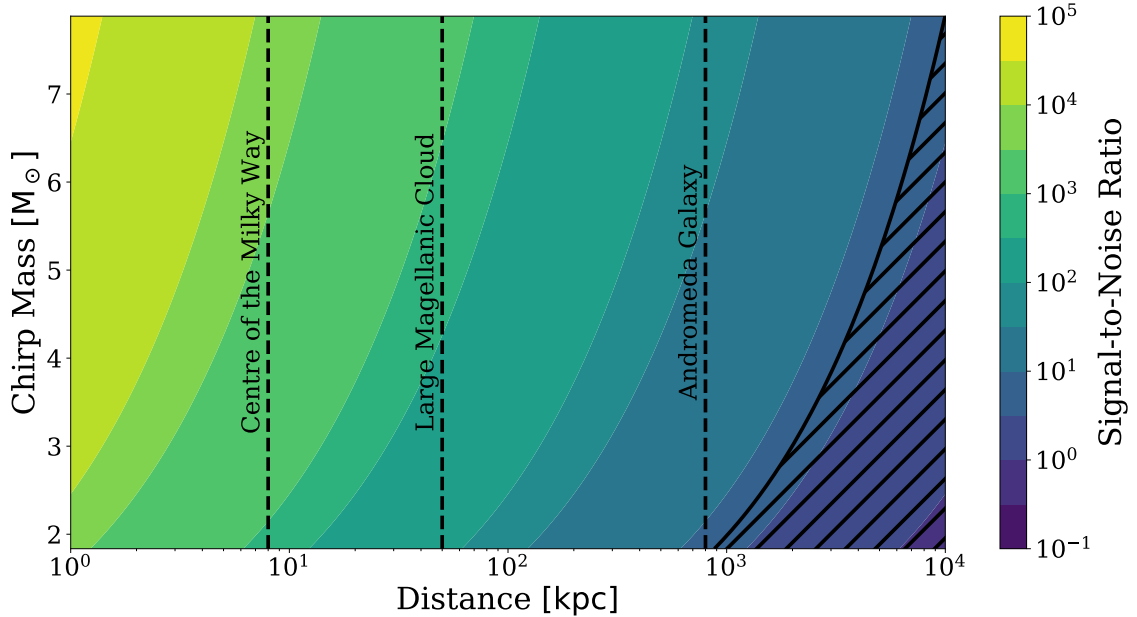
Figure 2.3: Signal-to-noise ratio for binary systems at the optimal frequency of $f \approx 4 \times 10^{-3}$ Hz. The chirp mass range is found by allowing neutron star masses between 1 and $3\,\mathrm{M_\odot}$ and black hole masses between 5 and $35\,\mathrm{M_\odot}$. The hashed area represents signal-to-noise ratios below 7, our pre-defined lower bound SNR for a detection. Therefore, all binaries in the hashed area are undetectable. The dashed black lines highlight the distances to nearby galaxies.

2.3 Time Observable in LISA Band

Although BH–NS binary systems with particular combinations of mass, frequency and distance may be theoretically detectable by LISA, only a small subfraction will be detectable during the LISA mission. This is because the binary systems form at different times in the history of our galaxy and will only be detectable in the LISA band for a small fraction of their lifetimes. Each BH–NS system will shrink in separation over time as orbital energy is lost through gravitational waves. This will cause an increase in frequency up to the point of merging and so LISA systems will process to the right in Fig. 2.2, and pass through the band.

2.3.1 Inspiral time

We estimate the fraction of systems detectable during the LISA mission by calculating the amount of time it takes a binary to pass through the frequency band. The inspiral time for a circular binary system is the amount of time it takes for the

system to merge since the formation of the BH–NS. The difference between the binary inspiral times at the minimum and maximum frequencies that LISA can detect gives the amount of time a binary spends in the LISA frequency band. The inspiral time is defined by Peters (1964) with

$$T_{\rm in}(a_0, m_1, m_2) = \frac{a_0^4}{4\beta(m_1, m_2)}, \tag{2.26}$$

where a_0 is the initial separation between the constituents of the binary system, the semi-major axis, and β is defined as

$$\beta(m_1, m_2) = \frac{64G^3}{5c^5}(m_1 m_2)(m_1 + m_2). \tag{2.27}$$

Through the application of Kepler's laws, we can write a simple relation between gravitational wave frequency, f and binary separation:

$$a = \left(\frac{G(m_1 + m_2)}{(\pi f)^2}\right)^{\frac{1}{3}}. \tag{2.28}$$

Combining the definition of a in equation 2.28 and $\mathcal{M}_c$ in equation 2.19 we can rewrite the insprial time in terms of chirp mass and gravitational wave frequency as

$$T_{\rm in}(\mathcal{M}_c, f) = \frac{5c^5}{256} \frac{1}{(G\mathcal{M}_c)^{\frac{5}{3}}(\pi f)^{\frac{8}{3}}}. \tag{2.29}$$

This function is plotted in Fig. 2.4 for the frequency range to which LISA is sensitive for our typical range of chirp masses. This plot illustrates the vast acceleration across frequency space. Systems at $f = 10^{-4}\,\mathrm{Hz}$ can take nearly a billion years to merge, while those at $f = 10^{-1}\,\mathrm{Hz}$ take under ten years and will sweep quickly out of the band. This demonstrates that we expect to find the majority of our sources at lower frequencies as the binary systems spend more time in these regions.

We can now also write the time spent in the LISA band, $T_{\rm obs}$, as a difference between the inspiral times at the endpoints of the LISA band (between 10^{-4} and
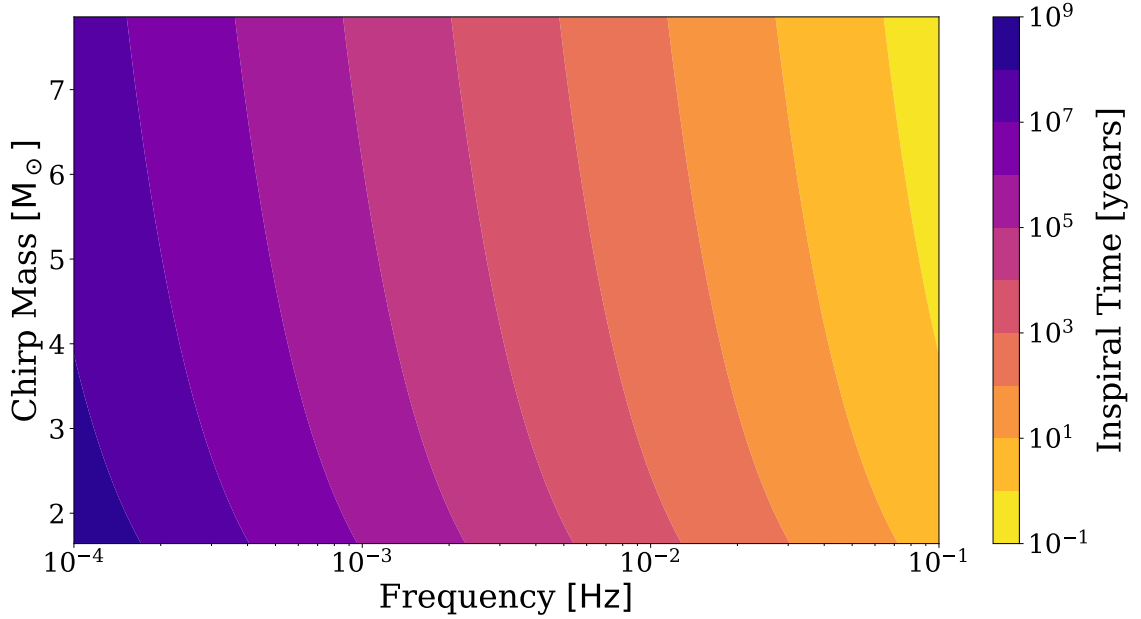
Figure 2.4: Inspiral time for binary systems across the LISA band for a range of LISA frequencies and BH–NS chirp masses. Systems at the far left of the band ($f \approx 10^{-4}\,\mathrm{Hz}$), taking nearly a billion years to merge, will appear stationary in frequency space on the timescale of the LISA mission. Systems at the far right ($f \approx 10^{-1}\,\mathrm{Hz}$), taking under ten years to merge, will move across the frequency space as LISA observes them and quickly move to LIGO's detection band.

10^{-1} Hz) for a typical binary.

$$T_{\mathrm{obs}} \approx 150\,\mathrm{Myr} \left(\frac{\mathcal{M}_c}{3M_\odot} \right)^{-\frac{5}{3}}. \tag{2.30}$$

As discussed in section 2.1.1, we assume that the galaxy is approximately $10\,\mathrm{Gyr}$ old. The fraction of BH–NS systems that are currently in the LISA band is the ratio of these timescales, given by

$$f_{\mathrm{LISA}} \approx 0.015 \left(\frac{\mathcal{M}_c}{3M_\odot} \right)^{-\frac{5}{3}}. \tag{2.31}$$

This reduces the number of systems in our galaxy that we expect to detect with LISA (equation 2.17) to approximately

$$N_{\mathrm{BHNS,LISA}} = N_{\mathrm{BHNS}} \cdot f_{\mathrm{LISA}} \approx 5700 \tag{2.32}$$

It is important to emphasise that this is an upper bound of the number of

detections. We have often assumed in these estimations that the system is currently at the optimal frequency for signal-to-noise and this will not be the case in reality. As we will show in our results, the majority of binaries lie around 10^{-4} Hz and spend very little time around the optimal frequency. This means that the detection rate for LISA is significantly lower than the result of these estimations.

However, the purpose of these estimations was only to ascertain whether there could exist *any* black hole neutron star binary that could be detected by LISA. We have shown that this is possible for systems in our galaxy and even nearby galaxies. We can now explore how many simulated systems exist in the detectable region of the parameter space and therefore establish how many detections we expect during LISA.

Chapter 3

Methods

3.1 BH–NS Population Synthesis with COMPAS

In order to simulate the evolution of a population of BH–NS binaries, we use simulations computed using the rapid population synthesis code COMPAS[1], performed by Broekgaarden et al. (in prep.). COMPAS is based on the algorithm presented in Tout, Aarseth, Pols, and Eggleton (1997), and this code includes single star evolution based on binary interactions by applying fitting formulae based on approximate prescriptions of the physical processes (Hurley, Pols, & Tout, 2000; Hurley, Tout, & Pols, 2002). The code has been used in a variety of works from modelling BBH to BNS (e.g. Stevenson et al., 2017; Vigna-Gómez et al., 2018b; Lau et al., 2020).

3.1.1 Sampling binaries in COMPAS

Using the COMPAS simulation they create 10^6 binaries by sampling from initial distributions of mass (for both binary components) and separation. They assume all stars have solar metallicity $Z = 0.0142$ at birth. They also make the assumption that each binary is circular at birth, but may become eccentric during BH–NS formation events, such as after the kick of either supernova. This assumption is not problematic compared to other uncertainties such as the common envelope phase,

---

[1]**C**ompact **O**bject **M**ergers: **P**opulation **A**strophysics and **S**tatistics, see https://compas.science/

since close binaries are expected to circularise by the first mass transfer and this analysis focusses on BH–NS systems, which are post mass transfer binaries (Zahn, 1977; Verbunt & Phinney, 1995; Belczyński & Bulik, 1999; Hurley et al., 2002).

They define the primary mass as the initially more massive component. This primary mass is drawn from the IMF defined in Kroupa (2001) (shown in Fig. 2.1). They consider only primary masses from 5 to $150 \, \mathrm{M_\odot}$ and a slope of $m^{-2.3}$ (the black region on Fig. 2.1). For the secondary mass, they assume a uniform distribution in mass ratio $q = m_2/m_1$ in $[0, 1]$ (Tout, 1991; Mazeh, Goldberg, Duquennoy, & Mayor, 1992; Goldberg & Mazeh, 1994). For the separation distribution, they use a flat-in-log distribution for $a \in [0.01, 1000] \, \mathrm{AU}$ (Öpik, 1924; Abt, 1983; Moe & Di Stefano, 2017).

BH–NS systems are rare in simulations and therefore if we were to simply draw randomly from these distributions we would find too small a population of BH–NS to make statistically significant calculations. Therefore, they use the adaptive importance sampling algorithm STROOPWAFEL, presented in Broekgaarden et al. (2019).

This algorithm improves the sampling of rare binary systems such as BH–NS systems by a factor of about 20-200 times compared to traditional Monte Carlo sampling. The algorithm starts by drawing random binaries from the birth distributions until it finds a sufficient population of BH–NS. It then uses these binaries to adapt the sampling distribution such that they draw more binaries from parameters near to those that created a BH–NS. Finally, using these updated sampling distributions, they continue to draw binaries at a higher sampling efficiency. Each sample is assigned a weight so that the predicted populations reflect the birth distributions.

3.1.2 Output Parameters

The COMPAS simulation produces a sample of BH–NS following the aforementioned algorithm. For each binary COMPAS determines several parameters from the simulation, each given in the Table 3.1.

Parameter	Description
M_1	Final compact object mass of initially more massive star
M_2	Final compact object mass of initially less massive star
a_0	Semi major axis at double compact object formation
e_0	Eccentricity at double compact object formation
t_{form}	Time to formation of double compact object
w	Weight assigned by the sampling algorithm STROOPWAFEL

Table 3.1: Table of parameters as DCO formation known for each binary produced by COMPAS simulation

3.1.3 Selecting a population of BH–NS for LISA

Using the sample of binaries that was created by Broekgaarden et al. (in prep.) using COMPAS, we now describe our analysis of this sample. We start by masking the binaries based on several criteria.

First, we require that the binary merges within a Hubble time. This ensures that the binary will merge within the age of our Universe and so pass through the LISA frequency band. Second, we reject any binaries in which one of the stars immediately fills its Roche Lobe after a common envelope event. This is because we assume that these stars will quickly merge into one star, without forming a compact binary and so will never be detectable by LISA as BH–NS sources.

Finally, we do not allow donor stars that are currently in the Hertzsprung-gap to survive a common envelope event. It is believed that these stars will not have developed a steep density gradient between their core and envelope (Taam & Sandquist, 2000; Ivanova & Taam, 2004) making it challenging to successfully eject the envelope. This follows the "pessimistic" scenario for the CE event used in other studies (e.g. Dominik et al., 2012; Giacobbo & Mapelli, 2018; Neijssel et al., 2019; Wiktorowicz et al., 2019). However, note that the label, "pessimistic" can be misleading, since it is unclear which scenario is more accurate.

3.1.4 Converting to a Milky Way Detection Rate

In order convert the synthesised binary population to a Milky Way population we need to make three main adjustments before it is representative of the Milky Way.

Firstly, as explained in section 3.1, the STROOPWAFEL algorithm amplifies the number of BH–NS binaries in the sample compared to the true rate in the Milky Way. The algorithm assigns a weight to each binary that represents how much it was amplified, such that a binary that was made twice as likely is given a weight of 0.5. Therefore, rather than counting the number of detectable binaries in the galaxy, we total the weights of the detectable binaries to account for the amplification. This makes the rate a factor of 100 times lower than without weights.

Moreover, the COMPAS simulation only considers a subpopulation of the underlying population of binaries. As mentioned in section 3.1.1, we only consider stars with masses of at least $5 \, \mathrm{M_\odot}$. Yet, from the Kroupa IMF (see Fig. 2.1), it is clear that there are *many* stars with mass less than $5 \, \mathrm{M_\odot}$. Therefore, we need to account for the fact that we only consider a subset of the parameter space when creating the population. Once we have a final detection rate for BH–NS binaries, we find the fraction of the parameter space that our simulation occupied and 'dilute' our rate by this fraction. This can be calculated by integrating the normalised IMF for the mass range, $[5, 150] \, \mathrm{M_\odot}$. This gives a fraction of 0.2 and so has the effect of lowering the rate by approximately 5 times when considering the entire population of binaries.

Finally, the population produced by COMPAS contains 10^6 binaries, each drawn from the mass distributions discussed in Section 3.1.1. Therefore the total mass of the sample is on the order of $10^8 \, \mathrm{M_\odot}$, which is much less than the mass of the Milky Way. Therefore, we re-scale our population synthesis mass to match the Milky Way, which increases the detection rate. This has the effect of increasing the rate by approximately a factor of 1000.

Overall, we can see that these adjustments will increase the detection rate by approximately a factor of 2 from the initial value.

3.2 Construction of Mock Milky Way

Each BH–NS in the mock Milky Way has a position and birth time and we assume that the Milky Way has been continuously forming stars over the course of its history. This means that we can sample random birth times uniformly across the age of the galaxy, which we assume to be $10\,\mathrm{Gyr}$. We define these birth times as t_{birth} and the time at which the system evolves into a double compact object as t_{DCO}. The difference between these times is the formation time, which we define as t_{form}.

In selecting the positions, we utilise the galactic position distributions and mass from McMillan (2011). We assume that the Milky Way is a one-component disk and follows the distribution

$$\rho_{\mathrm{d}}(R, z) = \frac{\Sigma_{\mathrm{d,0}}}{2 z_{\mathrm{d}}} \exp\left(-\frac{|z|}{z_{\mathrm{d}}} - \frac{R}{R_{\mathrm{d}}}\right), \tag{3.1}$$

where R is the radius, z is the height and $\Sigma_{\mathrm{d,0}}, z_{\mathrm{d}}, R_{\mathrm{d}}$ are constants given in McMillan (2011). We can convert this mass density function to a probability distribution in R by normalising and integrating over z and θ to find

$$P(r = R) = \frac{1}{R_{\mathrm{d}}} e^{-\frac{R}{R_{\mathrm{d}}}}. \tag{3.2}$$

In order to sample radii from this distribution, we perform inverse-CDF sampling by applying the principle of the Universality of the Uniform. This states that, given the inverse cumulative distribution function (CDF), the application of this function to a uniform random variable on $[0, 1]$ gives a random variable distributed in the same way as the probability distribution. Therefore, we integrate Eq. 3.2 to find the CDF

$$P(r \leq R) = 1 - e^{-\frac{R}{R_{\mathrm{d}}}}, \tag{3.3}$$

and invert Eq. 3.3 to find the inverse CDF

$$F_R^{-1}(u) = -R_d \ln(1 - u), \tag{3.4}$$

where u is a uniform $[0, 1]$ random variable. One can repeat the same exercise for $|z|$ and find a similar equation

$$F_{|z|}^{-1}(u) = -z_d \ln(1 - u), \tag{3.5}$$

which produces randomly distributed *absolute* scale heights. One can then assign each height a random sign to account for the absolute value sign in Eq. 3.1.

Using Eq. 3.4 and Eq. 3.5 each binary can be assigned a random radius and height. Finally, one can sample an angle θ from a uniform distribution on the interval $[0, 2\pi)$. With these three coordinates, we assign each binary a random position in the galaxy. An example of this random assignment is shown in Fig. 3.1, that shows the location of our BH–NS systems, both when viewed from, and above the galactic plane.
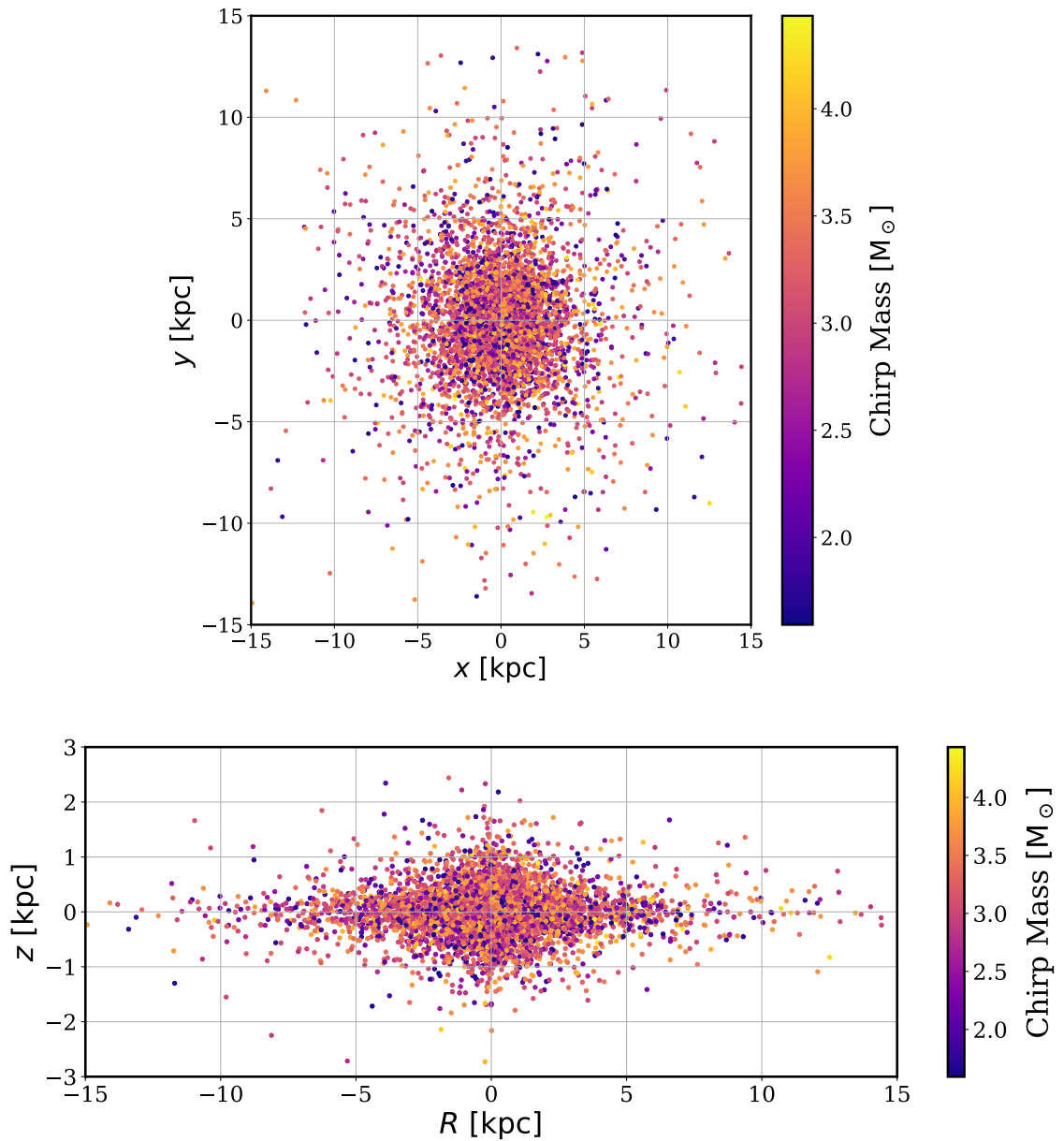
Figure 3.1: An example of randomised positions of BH–NS systems as used in this work, based on the Milky Way potential given in McMillan (2011). We calculate the positions and display the sample in two views where (a) shows the positions when looking down on the galactic plane, and (b) shows the positions when viewed from the galactic plane. The colour bars give an indication of the chirp mass of the binary system.

3.3 Orbital Decay

Since each BH–NS emits gravitational waves, which carry orbital energy away from the system, the BH–NS separation decreases (Peters, 1964). For circular orbits, this separation decay can be written as

$$a(t) = \left(a_0^4 - 4\beta t\right)^{1/4}, \tag{3.6}$$

where β is defined in Eq. 2.27. Eq. 3.6 shows that more massive systems will decay more quickly and each system will experience accelerated decay.

3.4 LISA Detection Rate Calculation

We can now summarise our method of calculating the BH–NS detection rate for the LISA mission. This is shown in Fig. 3.2 and explained below.

1. **Population Synthesis:** we use a simulation, performed by Broekgaarden et al. (in prep.), that produces a sample of compact binaries using the COMPAS code. We select the binaries of interest from this sample as described in section 3.1, such that we only take BH–NS systems that merge in a Hubble time.

2. **Milky Way Construction:** we assign each binary a random birth time, t_{birth}, between the start of the galaxy and the present day. Using the t_{form} parameter from COMPAS, we store the time at which the double compact object has formed as $t_{\mathrm{DCO}} = t_{\mathrm{birth}} + t_{\mathrm{form}}$. Additionally, we randomly assign each binary a position in the galaxy using the McMillan (2011) distribution, as explained in section 3.2.

3. **Binary Inspiral:** once each binary has been assigned a location and birth time, we can calculate its final separation at the time of the LISA mission. We use Eq. 3.6 to find the final separation, where a_0 is the separation produced by COMPAS and t is the time difference between t_{DCO} and $10\,\mathrm{Gyrs}$. For many binaries, this will result in a merger before LISA occurs and so we remove

them from this trial's sample at this point for efficiency.

4. **SNR Measurement:** Using the chirp mass, distance from Earth and final frequency (found by inverting Eq. 2.28) we calculate the signal-to-noise ratio for each binary using Eq. 2.25. As defined above, we use SNR= 7 as a threshold for detection and mark any binaries above this as detectable binaries.

5. **Repeat:** We repeat steps 2-4 25,000 times. For each repeat we assign each binary from the COMPAS simulation a new birth time and location in the Milky Way. We store the parameters of the detectable binaries from each repeat in addition to the number of detections.

6. **Adjustments:** finally, we now have an array of 25,000 counts of detectable binaries for each trial. However, we must adjust the value as discussed in section 3.1. Therefore, we apply the weights of each binary, account for the fact that we not simulate the whole parameter space and renormalise the mass using the mass of the Milky Way. After this, we define the detection rate to the be average value of this array.
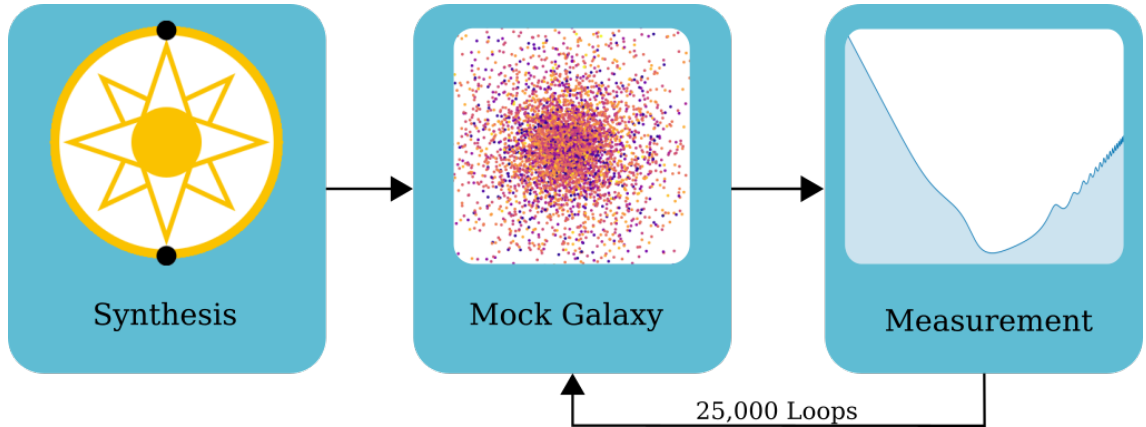
Figure 3.2: An illustration of our method for finding the detection rate of BH–NS in LISA. We start by using COMPAS to synthesise a population of BH–NS binaries. We then create a mock galaxy with these binaries and evolve them over the course of the Milky Way before measuring the SNR from each binary and storing those with SNR above our cutoff of 7. We repeat these steps 25,000 times and adjust the final total using the weights from STROOPWAFEL and renormalise the mass of the sample.

Chapter 4

Results

In this chapter we describe the results of our simulation for BH–NS evolution and detectability in LISA. We start by using 24128 binaries we find in our COMPAS simulation. After selecting the binaries of interest as described in section 3.1.3, we are left with a total sample of 6468 BH-NS binaries.

Fig. 4.1, similar to Fig. 2.2, illustrates the distributions of strain, SNR and frequency for BH–NS in the Milky Way. It shows the LISA sensitivity curve, overlaid with the sample of binaries. We plot only binaries with a sky averaged SNR greater than 10^{-4}, which represents approximately half of the sample. This figure shows that the majority of LISA BH–NS are at lower frequencies, in the yellow 'cloud' of points. This is because the inspiral time scales as $f^{-8/3}$ and so the binaries accelerate through frequency space. Therefore, binaries spend most time at lower frequencies and so we see them most often at lower frequencies. In comparison with our analytical estimations, we can see that every binary in the sample is below the optimal frequency of $f = 4 \times 10^{-3}$ Hz that we used in the estimations.
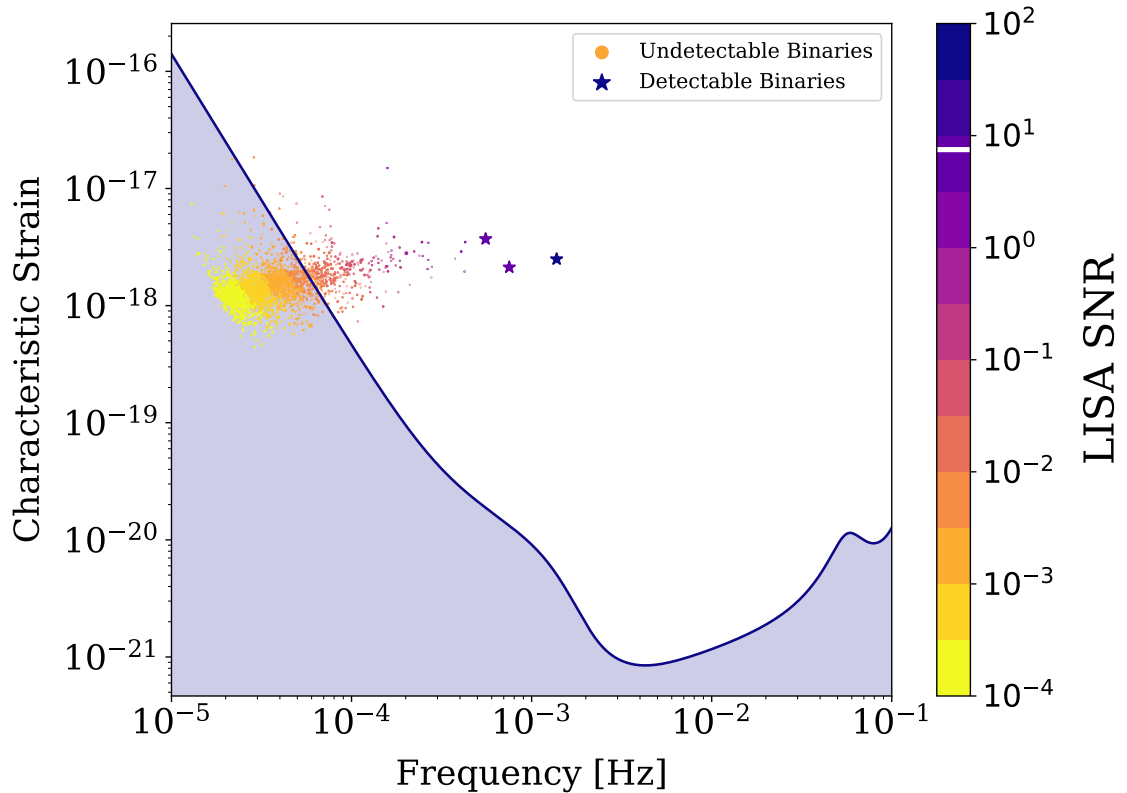
Figure 4.1: The SNR of a sample of BH–NS binaries from COMPAS scattered over the LISA sensitivity curve. Each point's size represents its weight and its colour represents its signal-to-noise ratio. Additionally, detectable binaries are shown as stars and their sizes have no relation to their weights. Note that we only plot binaries that have a signal-to-noise ratio of at least 10^{-4} (approximately half of the sample) The signal-to-noise ratio cutoff of 7 for detectability is marked with a white line on the colour bar.

4.1 Number of BH–NS detectable with LISA

We complete 25,000 trials of binary inspiral in the Milky Way and calculate a detection rate for each trial. After averaging these rates and adjusting as explained in section 3.1.4, we find the number of BH–NS binaries that we expect to detect during a four-year LISA mission is in the range

$$N_{\text{detect}} \in [0.0, 5.4], \tag{4.1}$$

enclosing 90% of the distribution and with a median number of detections of

$$\widetilde{N}_{\text{detect}} \approx 0.94 \pm 0.02, \tag{4.2}$$

where is the uncertainty is based on the statistical uncertainty from sampling. We note that the physical uncertainties are by far dominant over those resulting from sampling and may amount to multiple orders of magnitude (e.g. Dominik et al., 2012). The distribution of the number of detectable binaries is shown in Fig. 4.2. This figures shows that 90% of all repeats find between 0 and 5.6 BH–NS binaries. Therefore, if LISA were to detect a larger number of binaries than the median, such as 5, it does not necessarily rule out evolutionary models, but could in fact just be statistical fluctuations.
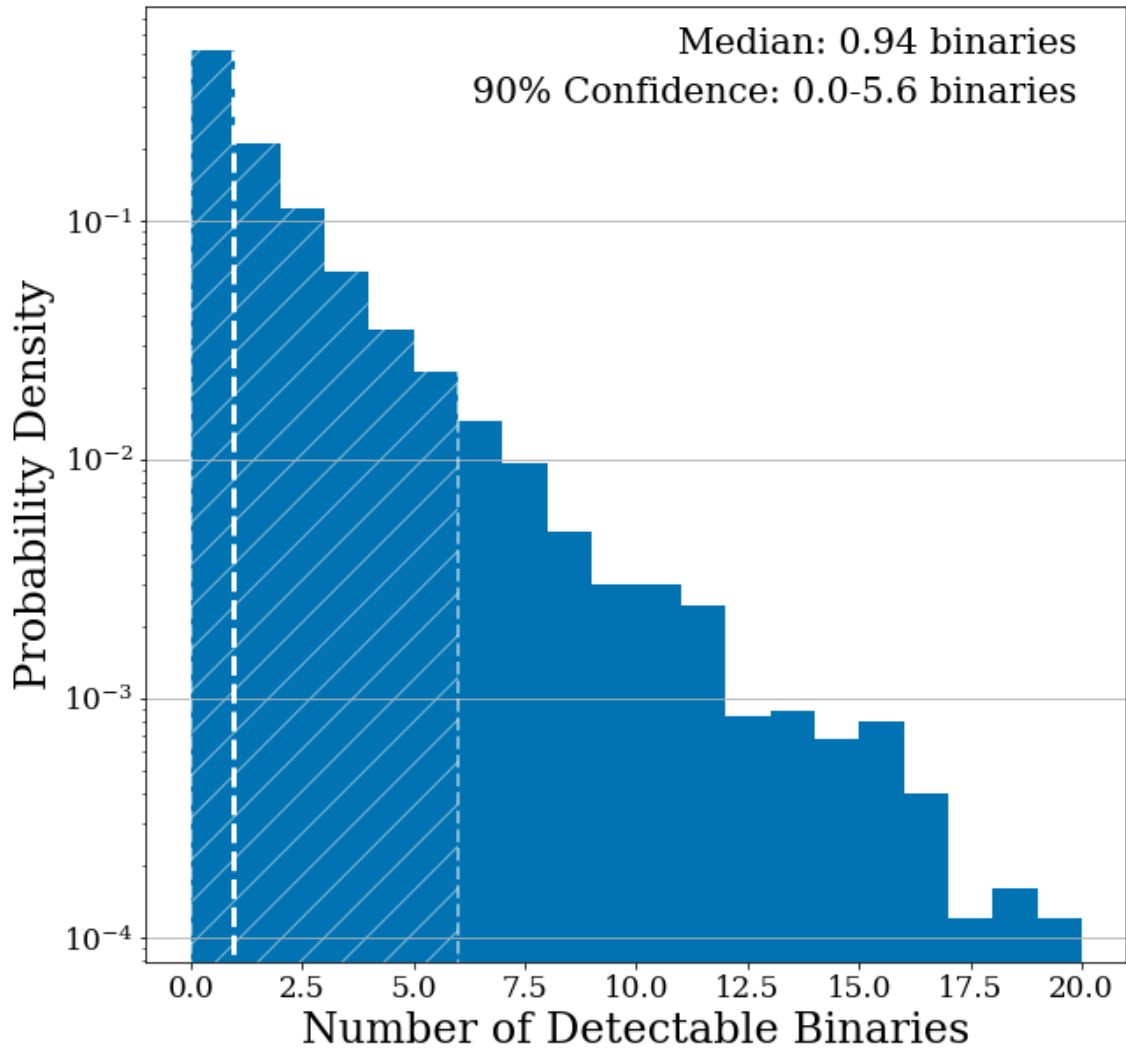
Figure 4.2: The distribution of detectable BH–NS systems over 25,000 bootstrapped BH–NS populations for our COMPAS simulation. The white dashedh line indicates the mean number of detectable binaries and the hashed area, enclosed by grey dashed lines, represents the central 90% of the distribution. We note that the majority of simulations result in fewer than 2 detectable binaries but the range extends as far as 20 detectable binaries.

4.2 Detectable BH–NS Binaries Characteristics

In this section, we show a series of comparisons for nine binary characteristics. As an initial distribution, we take the BH–NS binaries from the COMPAS sample that merge within a Hubble time. We then compare these with the distributions of all detectable binaries from the 25,000 trials. For each parameter we compute a kernel density estimator (KDE) to estimate the probability density function and show the distribution. Each KDE uses a bandwidth of 0.095.

Fig. 4.3 shows a grid of plots for each of the comparisons. For convenience, we also include enlarged, full page figures for each of the plots in Appendix A (figures A.1-A.8). We describe each of these plots in detail in the following sections and list the characteristics in Table 4.1.

Variable	Description	Details
m_{BH}	Black Hole Mass	Final mass of black hole
m_{NS}	Neutron Star Mass	Final mass of neutron star
$\mathcal{M}_{\mathrm{c}}$	Chirp Mass	Final chirp mass
f	Frequency	Frequency of emitted gravitational waves
a	Semi-major Axis	Binary orbit semi-major axis
d	Distance	Distance from Earth to binary
t_{form}	Formation Time	Time between birth and DCO formation
t_{DCO}	DCO Formation	Time at which DCO is formed
t_{c}	Coalescence Time	Time from DCO formation to merger

Table 4.1: A table of BH–NS characteristics that we examine in Fig. 4.3 and in Sections 4.2.1-4.2.6

4.2.1 Mass

In Fig. 4.3, the shape of the black hole mass distributions reflect the binary population results of COMPAS. There is a sharp cutoff at $M_{\mathrm{BH}} = 2.5\,\mathrm{M}_\odot$, which is in agreement with the COMPAS assumption that no black holes form with masses less than this threshold. Moreover, a majority of the black holes have masses greater than $10\,\mathrm{M}_\odot$. The distributions of detectable binaries and all binaries are similar, with a slight bias towards greater black hole masses for the detectable binaries as these have higher SNRs.
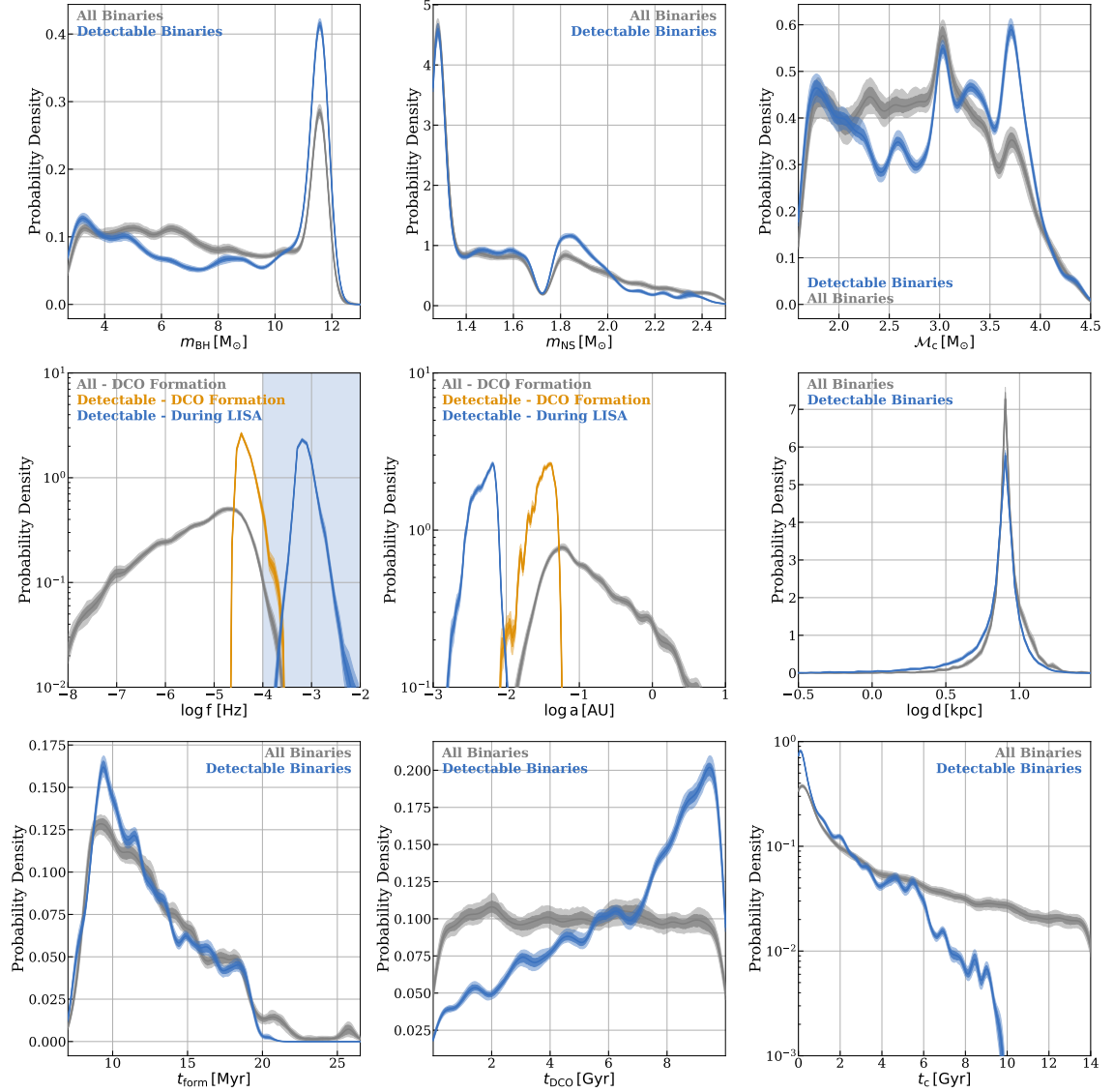
Figure 4.3: Characteristics of BH–NS binaries at DCO formation and during LISA. The grey kernel density estimators (KDE) represent the distribution of all BH–NS binaries in the COMPAS sample at the point of DCO formation. The blue KDEs represent the distribution of the BH–NS binaries that are detectable by LISA in any of the 25,000 repeats of Milky Way evolution. For frequency and separation, there is also an orange KDE, which represents the frequency (separation) at DCO formation, whilst the blue KDE still shows the distribution at the time of the LISA mission. The blue shaded region in the frequency plot represents the LISA frequency band. For each KDE, we also add shaded regions that represent the 1- and 2-σ uncertainties.

Similarly, for the neutron star mass, we can note several distinct features in the distributions. There is an excess of neutron star masses between 1.3 and 1.4 $M_\odot$. There is also a lack of neutron star masses around 1.7 $M_\odot$. This is a result of the discontinuity in the proto-compact object mass equation at carbon-oxygen cores of $M_{CO} = 3.5\,M_\odot$ (e.g. Fryer et al., 2012). This discontinuity is included in the COM-

PAS simulations and carries forward to affect the neutron star mass distribution.

Again we see that the two distributions are similar, with a slight bias towards greater neutron star masses for the detectable binaries.

For both distributions we see that detectable binaries skew towards greater masses and this is because the strain is larger for greater masses (Eq. 2.18) and so systems with a larger black hole or neutron star mass are more likely to be detectable.

Chirp Mass

In Fig. 4.3, we compare the distribution of chirp mass of all binaries in the sample that merge within a Hubble time to those binaries that are detectable by LISA. Since the chirp mass is a combination of the two component masses (see Eq. 2.19), we see that, similar to the black hole and neutron star mass distributions, the detectable binaries are skewed to higher masses.

4.2.2 Gravitational Wave Frequency

Fig. 4.3 shows that the initial distribution of frequencies of BH–NS binaries extend across many orders of magnitude, from 10^{-8}–10^{-4} Hz, but quickly drops off for frequencies above this range. If we compare this distribution to that of the detectable binaries at DCO formation, it is clear that higher frequencies are sharply favoured, with no detectable binaries found with frequencies lower than 10^{-5} Hz at DCO formation. The distribution of the frequencies during the LISA mission shifts to higher frequencies, approximately 10^{-4}–10^{-2} Hz, due to orbital decay (see Section 3.3)

The major factor that the distribution ends in this range is that, as we can see in Fig. 4.1, LISA is sensitive to frequencies approximately between 10^{-4}–10^{-1} Hz and it therefore makes sense that the detectable binaries are found in this frequency range. Moreover, a compounding factor is that we know from Eq. 2.18 that the strain scales with frequency as $f_{\mathrm{GW}}^{2/3}$ and so the strain is higher for a binary with higher orbital frequency.

4.2.3 BH–NS Binary Separation

Fig. 4.3 shows that the distribution of separation for all binaries at DCO formation is spread across 10^{-2}–10^2 AU but quickly drops off for separations outside of this range. If we compare this distribution to that of the detectable binaries at DCO formation, it is clear that smaller separations are sharply favoured. In particular, no detectable binaries are found with separations larger than 10^{-1} AU. These features are present for the same reasons as those in frequency since frequency and separation are directly related (see Eq. 2.28).

4.2.4 Distance

Fig. 4.3 shows the distribution of distances peaks around 8 kpc and drops off rapidly for lower distances. This is because in the density distribution that we use, most of the stars in the galaxy are concentrated around the centre, 8 kpc from the Earth. It is also notable that the distribution of detectable binaries is biased towards smaller distances. This is also expected, as we know from Eq. 2.18 that the strain is inversely proportional to distance. It is therefore easier to detect binaries that are closer.

4.2.5 Formation Time (t_{form})

The formation time is the difference between the birth of the stellar binary and the formation of the BH–NS, which is typically on the order of millions of years. Fig. 4.3 shows that the t_{form} distribution peaks around 10 Myr with a small spread, remaining within a factor of two of this peak. The distribution of all binaries and the distribution of detectable binaries are very similar, with only minor differences that can be attributed to statistical fluctuations.

4.2.6 Coalescence Time (t_{c})

Fig. 4.3 shows that the distribution of coalescence time for all binaries peaks around 1 Gyr, with the majority of binaries coalescing in fewer than 2 Gyr. There is then a

gradual dropoff for larger times with no clear cutoff.

The distribution of detectable binaries is skewed towards shorter coalescence times. From Eq. 2.26, we know that the coalescence time scales at a^4 for circular orbits and as we discussed above, the separations of detectable binaries are skewed towards smaller separations. Therefore, this explains the similar skew in coalescence times. There are no binaries detected with coalescence time greater than $10\,\mathrm{Gyr}$, our assumed age of the Milky Way. we are therefore artificially cutting off any binaries with larger coalescence times as they wouldn't merge in time for LISA to detect them.

Double Compact Object Birth Time (t_{DCO})

The double compact object birth time is time from the start of the Universe to the formation of the the BH–NS. Fig. 4.3 shows that the distribution of all binaries is approximately uniform across the age of the Milky Way. However, the distribution of detectable binaries demonstrates a clear correlation between detectability and birth time. There are many more detectable binaries that were born recently than at the start of the galaxy.

Upon comparison with the plot of coalescence time, this trend makes sense. We are most likely to detect binaries that have low separation since they produce the largest strains. However, the binary needs to have not merged before the LISA mission for us to detect it. So, since the most detectable binaries will be the closest to merging, and the coalescence time peaks below $2\,\mathrm{Gyr}$, we should detect mostly binaries from the past $2\,\mathrm{Gyr}$.

4.3   Comparison with other Studies

First, Lau et al. (2020) investigate the detectability of double neutron star (NS–NS) binaries with LISA. They find that LISA could detect 33 galactic NS–NS binaries over the course of a four-year mission.

If we repeat our calculation of the detection rate but instead select NS–NS binaries from the COMPAS population, we find that LISA will detect 5.3 NS–NS binaries over the course of a four-year mission. Lau et al. (2020) use the optimistic scenario of the common envelope phase and so we if change our assumptions to match this, we instead find 10.0 NS–NS binaries. This result is within a factor of 3 of the estimate given in the paper by Lau et al. (2020). As we will see in the next chapter, our assumption that all binaries are circular suppresses the rate by a factor of approximately 2-3 and we believe this may address the difference between our rate and that shown in Lau et al. (2020).

Another relevant study is Breivik et al. (2019), in which they investigate various LISA sources. They find that LISA will detect 31 Galactic BH–NS binaries over a four-year mission. This is a factor of 30 larger than our result.

We conclude that our results give lower estimates compared to above mentioned studies. This is mostly because of physical assumptions and the fact that this thesis does not consider the effects of eccentricity and this may explain the disagreement between our results.

4.4 Effects of Upgrading LISA on Detection Rate

The LISA mission is currently planned to last for four years but has a possible extension to ten years. In figure 4.4, we demonstrate the improvements in detection rates that we would gain from extending the mission. As a result of Eq. 2.25, the SNR increases in tandem with the observation time by a factor of roughly $\sqrt{2}$. Therefore, naturally a longer mission implies more detections since binary systems are pushed over the threshold of 7 SNR.
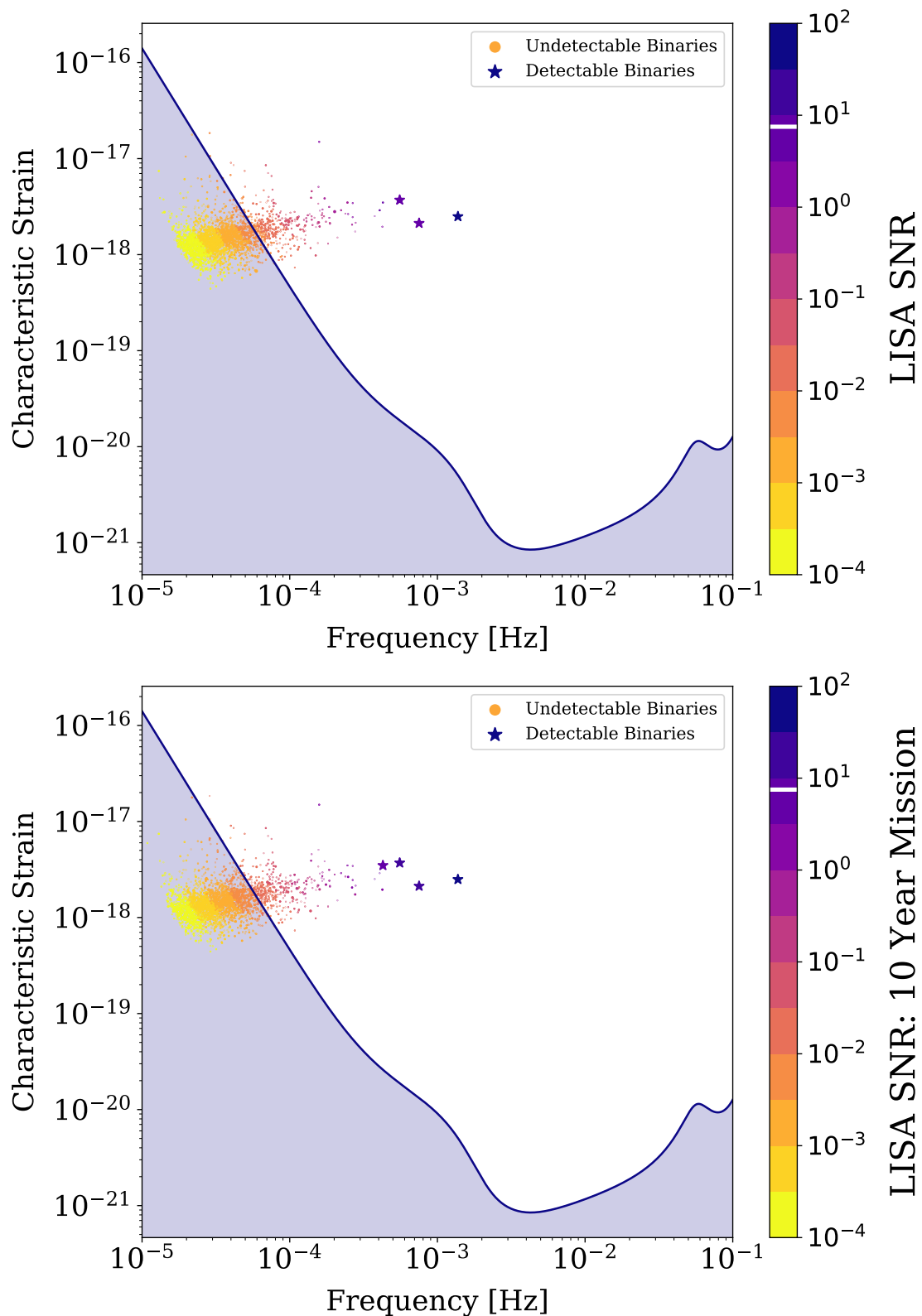
Figure 4.4: An illustration of the benefit of extending the LISA mission to 10 years. We see that extending the mission to ten years increases the number of detectable binaries and increases the signal-to-noise ratio of those that are undetectable.

4.5   Future Missions

Fig. 4.1 shows that the majority of BH–NS binaries are at lower frequencies than LISA can measure, therefore an instrument that is sensitive to lower frequency could lead to more detections. μ-Ares, a gravitational-wave detector proposed in Sesana et al. (2019). This detector would be sensitive to much lower frequencies, with a focus on microhertz frequencies, and so it may be more suitable for detecting BH–NS systems using this detector. Fig. 4.5 shows the distribution of simulated binaries for the μ-Ares mission. We see that this instrument would detect twice as many binaries as LISA and increase the average SNR significantly.
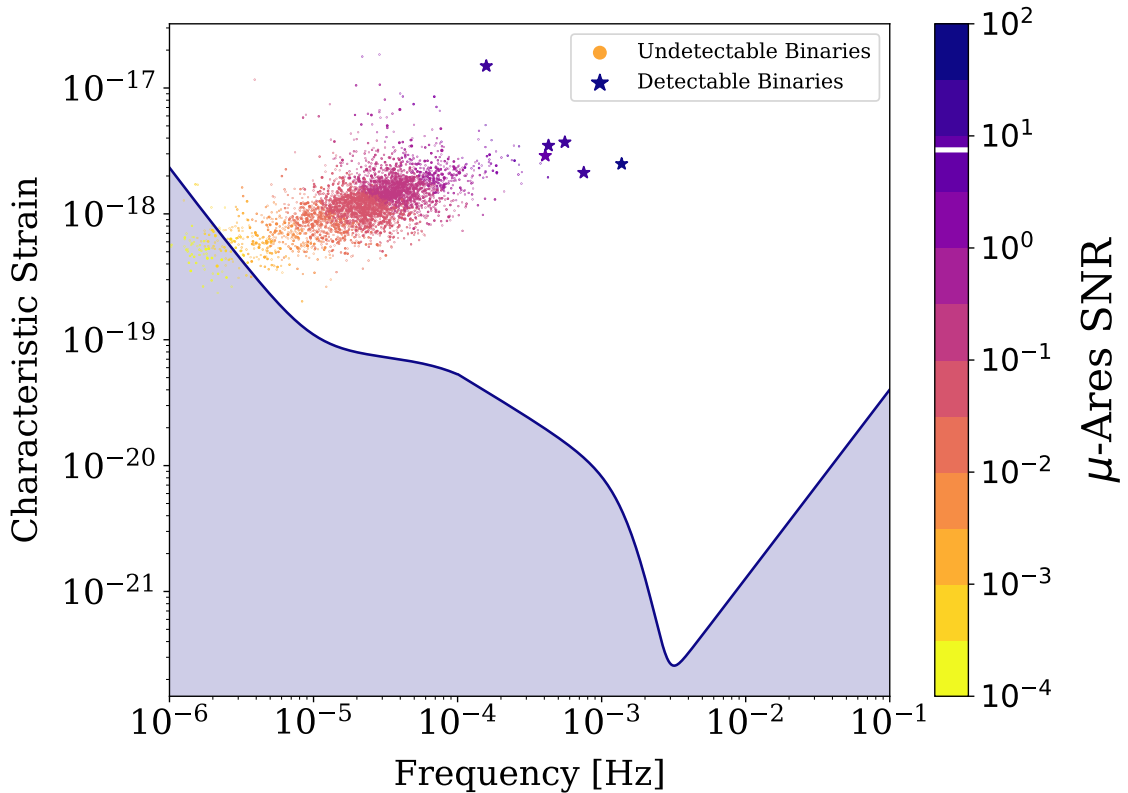
Figure 4.5: The SNR of a sample of binaries plotted with the sensitivity curve for the proposed μ-Ares detector, provided by Valeriya Korol, a postdoctoral fellow at the University of Birmingham. Note that these are the same binaries as Fig. 4.1 and Fig. 4.4. It is clear from the plot that the average SNR of the binaries is significantly higher. Moreover, 6 of the binary systems are now detectable, compared to 3 for a four-year LISA mission.

Mission	N_{detect}	$\widetilde{N}_{\mathrm{detect}}$	$\mathrm{P(N_{detect} \geq 1)}$
LISA 4 Years	[0, 5.4]	0.94 ± 0.02	48%
LISA 10 Years	[0, 7.4]	2.51 ± 0.02	69%
μ-Ares 10 Years	[0.5, 10.3]	4.24 ± 0.04	90%

Table 4.2: A comparison of the number of BH–NS that are detectable for different missions. Intervals span the central 90% of the distribution, the third column shows the median number of detections with statistical uncertainty and the last column is the probability that there is at least one detection over the course of the mission. The SNR is proportional to the square root of the observing time. Therefore, we see that the increase from extending the LISA mission is approximately equal to $\sqrt{10/4}$. Moreover, we note that the μ-Ares detector would be even more effective in detecting BH–NS binaries.

We compare the median number of detectable binaries between a four-year LISA mission, ten-year LISA mission and the μ-Ares mission in Table 4.2. Additionally, we plot the information given in Table 4.2 in Fig. 4.6.
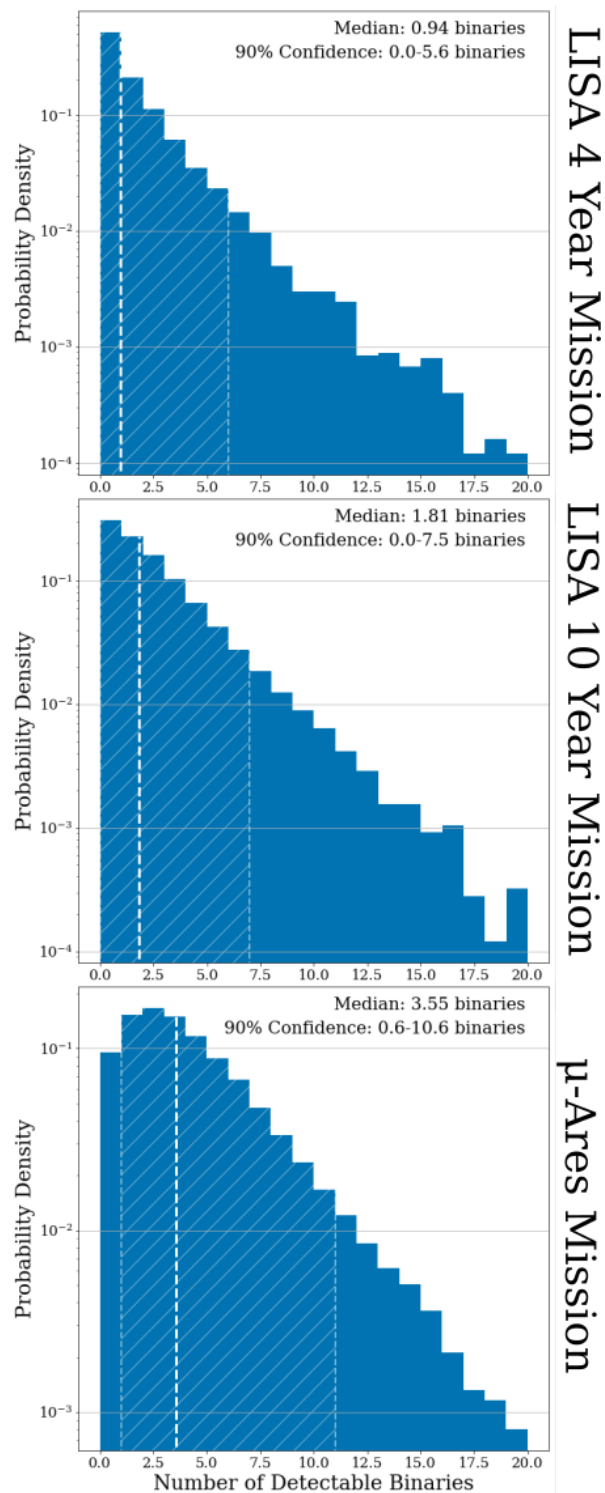
Figure 4.6: A comparison of the distribution of the number of detectable binaries for three different missions. Each plot shows the median with a dashed white line and the hatched area, enclosed by grey dashed lines represents the central 90% of the distribution.

Chapter 5

Discussion, Conclusion and Outlook

Based on the simulations presented in this work, we estimate between 0 and 5.4 detections of black hole neutron star binaries over the course of a four-year LISA mission. We made several assumptions and in this section we discuss their validity.

5.1 Model Considerations

5.1.1 Milky Way Star Formation Rate

For our model, we have assumed that the Milky Way has constant star formation at a rate of $6\,\mathrm{M_\odot}$ per year. The time at which a BH–NS binary forms is relevant to whether it can be detected. To take the extreme case, if all stars were formed in the past million years, then no binary would have the chance to inspiral and become detectable. Therefore, we should examine whether constant star formation is a sensible model.

An alternative to consider is starburst formation. In this case, all stars form in a single burst at one point in the history of the Milky Way. Studies such as Breivik et al. (2019) use this method and form their binaries from a single burst of star formation 13.7 Gyr ago.

However, recent studies into the star formation history of the Milky Way have clearly demonstrated that starburst formation is extremely unlikely (e.g. Snaith et al., 2015). Mor et al. (2019) argue that the Milky Way had a burst of star formation 2–3 Gyr ago and model the distribution as a combined exponential and gaussian (shown in figure 2 of their paper). With the size of the error bars, this trend is up for debate; it is possible to argue a continuous star formation history given the error bars (if we neglect the points from the past billion years). These studies therefore do not dissuade us from using a continuous star formation history.

5.1.2 Metallicity

Throughout our simulation, we assume that all BH–NS binaries orginate from progenitors for which we have assumed solar metallcity, irrespective of their birth time. The metallicity is important to our calculations since it has a strong effect on the mass loss rate by stellar winds (e.g. Maeder, 1992; Rolf P. Kudritzki, 2002; Belkus, Van Bever, & Vanbeveren, 2007; Mapelli & Bressan, 2013). In particular, for massive stars, stellar winds dominate mass loss and so increased stellar winds can affect the evolution of massive stars.

A lower metallicity implies that less mass is lost to stellar winds. For massive stars, this means that they will retain much more mass during evolution. Therefore, we would be more likely to form black holes and so more likely to form black hole–neutron star binaries.

Moreover, recent work by Laplace et al. (2020) showed that the expansion of stripped helium stars is strongly increased for lower metallicity. This may also increase the formation rate at lower metallicity.

Other studies, such as Breivik et al. (2019), use two different metallicities for comparison, in Breivik's case they use solar metallicity and 15% of solar metallicity.

5.1.3 Eccentricity

For our calculations we have assumed that all binaries in the sample are circular at DCO formation. When we create binaries with COMPAS we assume that all binaries start in a circular orbit. However, at the point of double compact object formation this may no longer be the case. For example, the supernovae that occur during formation can 'kick' the companion stars into eccentric orbits. For the sample of binaries produced by COMPAS, only approximately 2% of binaries have eccentricity below 0.1 at t_{DCO} and so it is likely a false assumption that binaries are circular.

In the next stages of this project, we will consider the effect of eccentricity on our calculations. This will alter several equations including Eq. 2.25, Eq. 2.28 and Eq. 3.6. From preliminary calculations, we estimate that this will increase the rate by a factor of roughly 2-3 times. It is also important to consider eccentricity as this will be measurable by LISA and be a useful tool in identifying and distinguishing characteristics of binaries.

5.1.4 Stationary Binaries

When we calculate the signal-to-noise ratio using Eq. 2.25, this is based on the assumption that the binaries are stationary in frequency space on the timescale of the LISA mission. If we use the mean frequency shown in the distribution in figure 4.3 and assume the length of the LISA mission is 4 years, then the rate of change of frequency, given in Peters (1964), scales as

$$\dot{f} = 1.4 \times 10^{-12} \, \frac{\mathrm{Hz}}{\mathrm{T_{obs}}} \left(\frac{T_{\mathrm{obs}}}{4 \, \mathrm{yr}} \right) \left(\frac{f}{1.1 \times 10^{-4} \, \mathrm{Hz}} \right)^{11/3} \left(\frac{\mathcal{M}_c}{3 \, \mathrm{M_\odot}} \right)^{5/3}, \qquad (5.1)$$

which shows that the frequency change is extremely minimal for the mean frequency binary in our sample. Moreover, if we use the maximum frequency of $1.4 \times 10^{-2} \, \mathrm{Hz}$, this still gives the rate of change as $7.3 \times 10^{-5} \, \frac{\mathrm{Hz}}{\mathrm{T_{obs}}}$, which is 0.52% change over the LISA mission. Therefore, we argue that it is a reasonable assumption that all binaries are stationary in frequency space on the timescale of the LISA mission.

5.2 Exploring BH–NS in other galaxies

We showed in section 2.2 that it is possible to detect BH–NS binaries as far as the Andromeda galaxy. Therefore, a natural extension of our calculations is to consider populations of binaries within other galaxies.

Future work should investigate the number of BH–NS binaries that can be detected in the Magellanic clouds and other galaxies. This can be done by assuming a population at one fixed distance to those galaxies and with a different metallicity. Note that for galaxies such as the LMC the metallicity will be significantly lower and this should boost detection rates in these galaxies as discussed in Section 5.1.2.

We expect the rates of detection from galaxies other than the Milky Way to be significantly lower since they are further away and less massive, but the decreased metallicity in other galaxies could balance these decreases to lead to a non-negligible detection rate in some other galaxies.

5.3 Distinguishing BH–NS binaries

In this thesis, we present a detection rate of BH–NS binaries for the LISA mission. However, this only means that we would *detect* a BH–NS signal, which is critically difference from *knowing* that we detected a BH–NS. It is difficult to distinguish gravitational wave signals and use them to find the parameters of the binary in LISA. This is because the binaries are stationary in the LISA band. For example, we could detect a BH–NS binary but confused it for a double neutron star or a double white dwarf.

In order to distinguish these types, one can use the chirp mass and mass ratio. Since, a BH–NS will have a significantly greater chirp mass than a double white dwarf, and the mass ratio q will be much smaller for a BH–NS than a double neutron star. However, it is not always easy to discern the mass from a gravitational wave signal in LISA, since for stationary binaries the chirp mass is degenerate with the distance to the source.

However, the possibility of a double white dwarf being detectable from another non-satellite galaxy is extremely small (e.g. Korol et al., 2020). Therefore, if we can confirm that a binary has been detected from far outside of the Milky Way then we can assume that this is not a double white dwarf. Although the distance is degenerate with chirp mass, if we can localise the binary on the sky then we can confirm whether the signal is coming from the direction of a nearby galaxy. This would allow us to rule out a double white dwarf. Then, if the binary was eccentric then we could find the mass ratio and distinguish between a BH–NS and double neutron star.

5.4 Summary and Conclusions

We have presented an estimate of the number of detectable BH–NS binaries for the LISA mission. While further studies will be necessary, the prospects for probing the properties of BH–NS binaries with LISA and using them as a tool for understanding our Universe is exciting. Depending on the number of binaries detected by LISA, we will be able to refine our models for massive stellar evolution and stellar remnants. If we happen to find several BH–NS binaries, then we can use them to clarify which types of black holes pair with which types of neutron stars and hone our understanding of BH–NS formation. Moreover, if we find a BH–NS in which the neutron star is a pulsar, we can use this to test general relativity and learn more about the nature of black holes. BH–NS binaries are exciting objects and their detection with LISA will help to refine many astrophysical theories.

Some key findings of our investigation are:

- Over the course of a four-year LISA mission, we expect to detect between 0 and 5 BH–NS binaries, with a 48% probability of having a least one detection (assuming a SNR threshold of 7).

- We find that for an extended LISA mission of ten years, these estimates increase to between 0 and 7 detectable BH–NS binaries and a 69% probability of detecting at least one. Moreover, μ-Ares would find between 0 and 10 sources and have a 90% probability of finding at least one.

- We demonstrate that, in principle, BH–NS binaries could be detected as far away as the Andromeda Galaxy and this could be used to distinguish them from double white dwarfs.

- We can use the number of BH–NS binaries that LISA detects to constrain and rule out models of massive stellar evolution.

Bibliography

Abbott, B. P., Abbott, R., Abbott, T. D., Abernathy, M. R., Acernese, F., Ackley, K., . . . Zweizig, J. (2016). Observation of gravitational waves from a binary black hole merger. *Phys. Rev. Lett.* 061102. doi:10.1103/PhysRevLett.116. 061102

Abt, H. A. (1983). Normal and abnormal binary frequencies. *Annual Review of Astronomy and Astrophysics*, *21*(1), 343–372. doi:10.1146/annurev.aa.21. 090183.002015. eprint: https://doi.org/10.1146/annurev.aa.21.090183.002015

Amaro-Seoane, P., Aoudia, S., Babak, S., Binétruy, P., Berti, E., Bohé, A., . . . Wardell, B. (2013). eLISA: Astrophysics and cosmology in the millihertz regime. *GW Notes*, *6*, 4–110. arXiv: 1201.3621 [astro-ph.CO]

Andrews, J. J., Breivik, K., Pankow, C., D'Orazio, D. J., & Safarzadeh, M. (2019). LISA and the Existence of a Fast-Merging Double Neutron Star Formation Channel. *arXiv e-prints*, arXiv:1910.13436. arXiv: 1910.13436 [astro-ph.HE]

Barrett, J. W., Gaebel, S. M., Neijssel, C. J., Vigna-Gómez, A., Stevenson, S., Berry, C. P. L., . . . Mandel, I. (2018). Accuracy of inference on the physics of binary evolution from gravitational-wave observations. *Monthly Notices of the RAS*, *477*(4), 4685–4695. doi:10.1093/mnras/sty908. arXiv: 1711.06287 [astro-ph.HE]

Belczynski, K., Benacquista, M., & Bulik, T. (2010). Double Compact Objects as Low-frequency Gravitational Wave Sources. *Astrophysical Journal*, *725*(1), 816–823. doi:10.1088/0004-637X/725/1/816. arXiv: 0811.1602 [astro-ph]

Belczyński, K., & Bulik, T. (1999). The effect of supernova natal kicks on compact object merger rate. *Astronomy and Astrophysics, 346*, 91–100. arXiv: astro-ph/9901193 [astro-ph]

Belczynski, K., Kalogera, V., Rasio, F. A., Taam, R. E., Zezas, A., Bulik, T., ... Ivanova, N. (2008). Compact Object Modeling with the StarTrack Population Synthesis Code. *Astrophysical Journal, Supplement, 174*(1), 223–260. doi:10.1086/521026. arXiv: astro-ph/0511811 [astro-ph]

Belkus, H., Van Bever, J., & Vanbeveren, D. (2007). The Evolution of Very Massive Stars. *Astrophysical Journal, 659*(2), 1576–1581. doi:10.1086/512181. arXiv: astro-ph/0701334 [astro-ph]

Błaut, A., Babak, S., & Królak, A. (2010). Mock LISA data challenge for the Galactic white dwarf binaries. *Physical Review D, 81*(6), 063008. doi:10.1103/PhysRevD.81.063008. arXiv: 0911.3020 [gr-qc]

Breivik, K., Coughlin, S. C., Zevin, M., Rodriguez, C. L., Kremer, K., Ye, C. S., ... Rasio, F. A. (2019). COSMIC Variance in Binary Population Synthesis. *arXiv e-prints*, arXiv:1911.00903. arXiv: 1911.00903 [astro-ph.HE]

Broekgaarden, F. S., Justham, S., de Mink, S. E., Gair, J., Mandel, I., Stevenson, S., ... Neijssel, C. J. (2019). STROOPWAFEL: simulating rare outcomes from astrophysical populations, with application to gravitational-wave sources. *Monthly Notices of the RAS, 490*(4), 5228–5248. doi:10.1093/mnras/stz2558. arXiv: 1905.00910 [astro-ph.HE]

Crowder, J., & Cornish, N. J. (2007). Solution to the galactic foreground problem for LISA. *Physical Review D, 75*(4), 043008. doi:10.1103/PhysRevD.75.043008. arXiv: astro-ph/0611546 [astro-ph]

Danzmann, K., & Rüdiger, A. (2003). LISA technology - concept, status, prospects. *Classical and Quantum Gravity, 20*(10), S1–S9. doi:10.1088/0264-9381/20/10/301

Dominik, M., Belczynski, K., Fryer, C., Holz, D. E., Berti, E., Bulik, T., . . . O'Shaughnessy, R. (2012). Double Compact Objects. I. The Significance of the Common Envelope on Merger Rates. *Astrophysical Journal*, *759*, 52.

Farr, W. M., Sravan, N., Cantrell, A., Kreidberg, L., Bailyn, C. D., Mandel, I., & Kalogera, V. (2011). The Mass Distribution of Stellar-mass Black Holes. *Astrophysical Journal*, *741*, 103.

Figer, D. F. (2005). An upper limit to the masses of stars. *Nature*, *434*(7030), 192–194. doi:10.1038/nature03293. arXiv: astro-ph/0503193 `[astro-ph]`

Finn, L. S., & Thorne, K. S. (2000). Gravitational waves from a compact star in a circular, inspiral orbit, in the equatorial plane of a massive, spinning black hole, as observed by LISA. *Phys. Rev. D*, *62*(12), 124021. doi:10.1103/PhysRevD.62.124021. arXiv: gr-qc/0007074 `[gr-qc]`

Flannery, B. P., & van den Heuvel, E. P. J. (1975). On the origin of the binary pulsar PSR 1913+16. *Astronomy and Astrophysics*, *39*, 61–67.

Fryer, C. L., Belczynski, K., Wiktorowicz, G., Dominik, M., Kalogera, V., & Holz, D. E. (2012). Compact Remnant Mass Function: Dependence on the Explosion Mechanism and Metallicity. *Astrophysical Journal*, *749*(1), 91. doi:10.1088/0004-637X/749/1/91. arXiv: 1110.1726 `[astro-ph.SR]`

Giacobbo, N., & Mapelli, M. [Michela]. (2018). The progenitors of compact-object binaries: impact of metallicity, common envelope and natal kicks. *Monthly Notices of the RAS*, *480*(2), 2011–2030. doi:10.1093/mnras/sty1999. arXiv: 1806.00001 `[astro-ph.HE]`

Goldberg, D., & Mazeh, T. [T.]. (1994). The mass-ratio distribution of the spectroscopic binaries in the Pleiades. *Astronomy and Astrophysics*, *282*, 801–803.

Heger, A., Fryer, C. L., Woosley, S. E., Langer, N., & Hartmann, D. H. (2003). How Massive Single Stars End Their Life. *Astrophysical Journal*, *591*(1), 288–300. doi:10.1086/375341. arXiv: astro-ph/0212469 `[astro-ph]`

Hurley, J. R., Pols, O. R., & Tout, C. A. (2000). Comprehensive analytic formulae for stellar evolution as a function of mass and metallicity. *Monthly Notices*

of the RAS, *315*(3), 543–569. doi:10.1046/j.1365-8711.2000.03426.x. arXiv: astro-ph/0001295 [astro-ph]

Hurley, J. R., Tout, C. A., & Pols, O. R. (2002). Evolution of binary stars and the effect of tides on binary populations. *Monthly Notices of the Royal Astronomical Society*, *329*(4), 897–928. doi:10.1046/j.1365-8711.2002.05038.x. eprint: https://academic.oup.com/mnras/article-pdf/329/4/897/18418535/329-4-897.pdf

Ivanova, N., & Taam, R. E. (2004). Thermal timescale mass transfer and the evolution of white dwarf binaries. *The Astrophysical Journal*, *601*(2), 1058–1066. doi:10.1086/380561

Kasper, M., Biller, B. A., Burrows, A., Brandner, W., Budaj, J., & Close, L. M. (2007). The very nearby M/T dwarf binary SCR 1845-6357. *Astronomy and Astrophysics*, *471*(2), 655–659. doi:10.1051/0004-6361:20077881. arXiv: 0706.3824 [astro-ph]

Korol, V., Toonen, S., Klein, A., Belokurov, V., Vincenzo, F., Buscicchio, R., . . . Vecchio, A. (2020). Populations of double white dwarfs in Milky Way satellites and their detectability with LISA. *arXiv e-prints*, arXiv:2002.10462. arXiv: 2002.10462 [astro-ph.GA]

Kroupa, P. (2001). On the variation of the initial mass function. *MNRAS*, *322*(2), 231–246. doi:10.1046/j.1365-8711.2001.04022.x. arXiv: astro-ph/0009005 [astro-ph]

Kruckow, M. U., Tauris, T. M., Langer, N., Kramer, M., & Izzard, R. G. (2018). Progenitors of gravitational wave mergers: binary evolution with the stellar grid-based code COMBINE. *Monthly Notices of the RAS*, *481*(2), 1908–1949. doi:10.1093/mnras/sty2190. arXiv: 1801.05433 [astro-ph.SR]

Kudritzki, R. P. [R. P.], Pauldrach, A., & Puls, J. (1987). Radiation driven winds of hot luminous stars. II. Wind models for O-stars in the Magellanic clouds. *Astronomy and Astrophysics*, *173*, 293–298.

Kudritzki, R. P. [Rolf P.]. (2002). Line-driven Winds, Ionizing Fluxes, and Ultraviolet Spectra of Hot Stars at Extremely Low Metallicity. I. Very Massive O Stars. *Astrophysical Journal*, *577*(1), 389–408. doi:10.1086/342178. arXiv: astro-ph/0205210 [astro-ph]

Kudritzki, R.-P., & Puls, J. (2000). Winds from Hot Stars. *Annual Review of Astrononomy and Astrophysics*, *38*, 613–666. doi:10.1146/annurev.astro.38.1.613

Lamberts, A., Blunt, S., Littenberg, T. B., Garrison-Kimmel, S., Kupfer, T., & Sanderson, R. E. (2019). Predicting the LISA white dwarf binary population in the Milky Way with cosmological simulations. *Monthly Notices of the RAS*, *490*(4), 5888–5903. doi:10.1093/mnras/stz2834. arXiv: 1907.00014 [astro-ph.HE]

Laplace, E., Götberg, Y., de Mink, S. E., Justham, S., & Farmer, R. (2020). The expansion of stripped-envelope stars: consequences for supernovae and gravitational-wave progenitors. *arXiv e-prints*, arXiv:2003.01120. arXiv: 2003.01120 [astro-ph.SR]

Lau, M. Y. M., Mandel, I., Vigna-Gómez, A., Neijssel, C. J., Stevenson, S., & Sesana, A. (2020). Detecting double neutron stars with LISA. *Monthly Notices of the RAS*, *492*(3), 3061–3072. doi:10.1093/mnras/staa002. arXiv: 1910.12422 [astro-ph.HE]

Leitherer, C., Robert, C., & Drissen, L. (1992). Deposition of Mass, Momentum, and Energy by Massive Stars into the Interstellar Medium. *Astrophysical Journal*, *401*, 596. doi:10.1086/172089

Licquia, T. C., & Newman, J. A. (2015). Improved Estimates of the Milky Way's Stellar Mass and Star Formation Rate from Hierarchical Bayesian Meta-Analysis. *APJ*, *806*(1), 96. doi:10.1088/0004-637X/806/1/96. arXiv: 1407.1078 [astro-ph.GA]

Maeder, A. (1992). Stellar yields as a function of initial metallicity and mass limit for black hole formation. *Astronomy and Astrophysics*, *264*(1), 105–120.

Mapelli, M. [M.], & Bressan, A. (2013). Impact of metallicity on the evolution of young star clusters. *Monthly Notices of the RAS*, *430*(4), 3120–3127. doi:10.1093/mnras/stt119. arXiv: 1301.4227 [astro-ph.GA]

Mazeh, T. [Tsevi], Goldberg, D., Duquennoy, A., & Mayor, M. (1992). On the Mass-Ratio Distribution of Spectroscopic Binaries with Solar-Type Primaries. *Astrophysical Journal*, *401*, 265. doi:10.1086/172058

McMillan, P. J. (2011). Mass models of the Milky Way. *MNRAS*, *414*(3), 2446–2457. doi:10.1111/j.1365-2966.2011.18564.x. arXiv: 1102.4340 [astro-ph.GA]

Moe, M., & Di Stefano, R. (2017). Mind Your Ps and Qs: The Interrelation between Period (P) and Mass-ratio (Q) Distributions of Binary Stars. *APJS*, *230*(2), 15. doi:10.3847/1538-4365/aa6fb6. arXiv: 1606.05347 [astro-ph.SR]

Mor, R., Robin, A. C., Figueras, F., Roca-Fàbrega, S., & Luri, X. (2019). Gaia DR2 reveals a star formation burst in the disc 2-3 Gyr ago. *Astronomy and Astrophysics*, *624*, L1. doi:10.1051/0004-6361/201935105. arXiv: 1901.07564 [astro-ph.GA]

Neijssel, C. J., Vigna-Gómez, A., Stevenson, S., Barrett, J. W., Gaebel, S. M., Broekgaarden, F. S., . . . Mandel, I. (2019). The effect of the metallicity-specific star formation history on double compact object mergers. *Monthly Notices of the RAS*, *490*(3), 3740–3759. doi:10.1093/mnras/stz2840. arXiv: 1906.08136 [astro-ph.SR]

Nelemans, G., Yungelson, L. R., & Portegies Zwart, S. F. (2001). The gravitational wave signal from the Galactic disk population of binaries containing two compact objects. *Astronomy and Astrophysics*, *375*, 890–898. doi:10.1051/0004-6361:20010683. arXiv: astro-ph/0105221 [astro-ph]

Nelemans, G., Yungelson, L. R., & Portegies Zwart, S. F. (2004). Short-period AM CVn systems as optical, X-ray and gravitational-wave sources. *Monthly Notices of the RAS*, *349*(1), 181–192. doi:10.1111/j.1365-2966.2004.07479.x. arXiv: astro-ph/0312193 [astro-ph]

Öpik, E. (1924). Statistical Studies of Double Stars: On the Distribution of Relative Luminosities and Distances of Double Stars in the Harvard Revised Photometry North of Declination -31 degrees. *Publications of the Tartu Astrofizica Observatory*, *25*, 1.

Pauldrach, A. W. A., Vanbeveren, D., & Hoffmann, T. L. (2012). Radiation-driven winds of hot luminous stars XVI. Expanding atmospheres of massive and very massive stars and the evolution of dense stellar clusters. *Astronomy and Astrophysics*, *538*, A75. doi:10.1051/0004-6361/201117621. arXiv: 1107.0654 [astro-ph.SR]

Peters, P. C. (1964). Gravitational Radiation and the Motion of Two Point Masses. *Physical Review*, *136*(4B), 1224–1232. doi:10.1103/PhysRev.136.B1224

Portinari, L., Chiosi, C., & Bressan, A. (1998). Galactic chemical enrichment with new metallicity dependent stellar yields. *Astronomy and Astrophysics*, *334*, 505–539. arXiv: astro-ph/9711337 [astro-ph]

Renzo, M., Zapartas, E., de Mink, S. E., Götberg, Y., Justham, S., Farmer, R. J., . . . Sana, H. (2019). Massive runaway and walkaway stars. A study of the kinematical imprints of the physical processes governing the evolution and explosion of their binary progenitors. *Astronomy and Astrophysics*, *624*, A66. doi:10.1051/0004-6361/201833297. arXiv: 1804.09164 [astro-ph.SR]

Robson, T., Cornish, N. J., & Liu, C. (2019). The construction and use of LISA sensitivity curves. *Classical and Quantum Gravity*, *36*(10), 105011. doi:10.1088/1361-6382/ab1101. arXiv: 1803.01944 [astro-ph.HE]

Robson, T., Cornish, N. J., Tamanini, N., & Toonen, S. (2018). Detecting hierarchical stellar systems with LISA. *Physical Review D*, *98*(6), 064012. doi:10.1103/PhysRevD.98.064012. arXiv: 1806.00500 [gr-qc]

Sana, H., de Mink, S. E., de Koter, A., Langer, N., Evans, C. J., Gieles, M., . . . Schneider, F. R. N. (2012). Binary Interaction Dominates the Evolution of Massive Stars. *Science*, *337*(6093), 444. doi:10.1126/science.1223344. arXiv: 1207.6397 [astro-ph.SR]

Sesana, A., Korsakova, N., Arca Sedda, M., Baibhav, V., Barausse, E., Barke, S., . . .
Zumalacarregui, M. (2019). Unveiling the Gravitational Universe at μ-Hz Frequencies. *arXiv e-prints*, arXiv:1908.11391. arXiv: 1908.11391 [astro-ph.IM]

Smarr, L. L., & Blandford, R. (1976). The binary pulsar: physical processes, possible companions, and evolutionary histories. *Astrophysical Journal*, *207*, 574–588. doi:10.1086/154524

Snaith, O., Haywood, M., Di Matteo, P., Lehnert, M. D., Combes, F., Katz, D., & Gómez, A. (2015). Reconstructing the star formation history of the Milky Way disc(s) from chemical abundances. *Astronomy and Astrophysics*, *578*, A87. doi:10.1051/0004-6361/201424281. arXiv: 1410.3829 [astro-ph.GA]

Srinivasan, G. (1989). Pulsars: their origin and evolution. *Astronomy and Astrophysics Reviews*, *1*(3-4), 209–260. doi:10.1007/BF00873079

Stevenson, S., Vigna-Gómez, A., Mandel, I., Barrett, J. W., Neijssel, C. J., Perkins, D., & de Mink, S. E. (2017). Formation of the first three gravitational-wave observations through isolated binary evolution. *Nature Communications*, *8*, 14906. doi:10.1038/ncomms14906. arXiv: 1704.01352 [astro-ph.HE]

Sukhbold, T., Ertl, T., Woosley, S. E., Brown, J. M., & Janka, H. .-.-T. (2016). Core-collapse Supernovae from 9 to 120 Solar Masses Based on Neutrino-powered Explosions. *Astrophysical Journal*, *821*(1), 38. doi:10.3847/0004-637X/821/1/38. arXiv: 1510.04643 [astro-ph.HE]

Taam, R. E., & Sandquist, E. L. (2000). Common Envelope Evolution of Massive Binary Stars. *Annual Review of Astrononomy and Astrophysics*, *38*, 113–141. doi:10.1146/annurev.astro.38.1.113

Tamanini, N., & Danielski, C. (2019). The gravitational-wave detection of exoplanets orbiting white dwarf binaries using LISA. *Nature Astronomy*, *3*, 858–866. doi:10.1038/s41550-019-0807-y. arXiv: 1812.04330 [astro-ph.EP]

Tauris, T. M., Kramer, M., Freire, P. C. C., Wex, N., Janka, H. .-.-T., Langer, N., . . . Champion, D. J. (2017). Formation of Double Neutron Star Sys-

tems. *APJ*, *846*(2), 170. doi:10.3847/1538-4357/aa7e89. arXiv: 1706.09438
[astro-ph.HE]

Tauris, T. M., & van den Heuvel, E. P. J. (2006). Formation and evolution of compact
stellar X-ray sources. In *Compact stellar x-ray sources* (Vol. 39, pp. 623–665).

Tout, C. A. (1991). On the relation between the mass-ratio distribution in binary
stars and the mass function for single stars. *Monthly Notices of the RAS*, *250*,
701–706. doi:10.1093/mnras/250.4.701

Tout, C. A., Aarseth, S. J., Pols, O. R., & Eggleton, P. P. (1997). Rapid binary star
evolution for N-body simulations and population synthesis. *Monthly Notices
of the RAS*, *291*(4), 732–748. doi:10.1093/mnras/291.4.732

Verbunt, F., & Phinney, E. S. (1995). Tidal circularization and the eccentricity of
binaries containing giant stars. *Astronomy and Astrophysics*, *296*, 709.

Vigna-Gómez, A., MacLeod, M., Neijssel, C. J., Broekgaarden, F. S., Justham, S.,
Howitt, G., ... Mand el, I. (2020). Common-Envelope Episodes that lead
to Double Neutron Star formation. *arXiv e-prints*, arXiv:2001.09829. arXiv:
2001.09829 [astro-ph.SR]

Vigna-Gómez, A., Neijssel, C. J., Stevenson, S., Barrett, J. W., Belczynski, K.,
Justham, S., ... Mandel, I. (2018a). On the formation history of Galactic dou-
ble neutron stars. *MNRAS*, *481*(3), 4009–4029. doi:10.1093/mnras/sty2463.
arXiv: 1805.07974 [astro-ph.SR]

Vigna-Gómez, A., Neijssel, C. J., Stevenson, S., Barrett, J. W., Belczynski, K.,
Justham, S., ... Mandel, I. (2018b). On the formation history of Galactic
double neutron stars. *Monthly Notices of the RAS*, *481*(3), 4009–4029. doi:10.
1093/mnras/sty2463. arXiv: 1805.07974 [astro-ph.SR]

Vink, J. S., de Koter, A., & Lamers, H. J. G. L. M. (2001). Mass-loss predictions
for O and B stars as a function of metallicity. *Astronomy and Astrophysics*,
369, 574–588. doi:10.1051/0004-6361:20010127. arXiv: astro-ph/0101509
[astro-ph]

Wellstein, S., Langer, N., & Braun, H. (2001). Formation of contact in massive close binaries. *AAP*, *369*, 939–959. doi:10.1051/0004-6361:20010151. arXiv: astro-ph/0102244 [astro-ph]

Wiktorowicz, G., Wyrzykowski, Ł., Chruslinska, M., Klencki, J., Rybicki, K. A., & Belczynski, K. (2019). Populations of Stellar-mass Black Holes from Binary Systems. *Astrophysical Journal*, *885*(1), 1. doi:10.3847/1538-4357/ab45e6. arXiv: 1907.11431 [astro-ph.HE]

Zahn, J. .-.-P. (1977). Reprint of 1977A&A....57..383Z. Tidal friction in close binary stars. *Astronomy and Astrophysics*, *500*, 121–132.

Appendices

Appendix A

Binary Parameter Comparisons

This appendix contains full page plots of the grid of plots shown in Fig. 4.3. These plots compare the distributions of binary parameters for all binaries that merge within a Hubble time and binaries that are detectable with LISA. Each plot is discussed in more detail in Section 4.2.
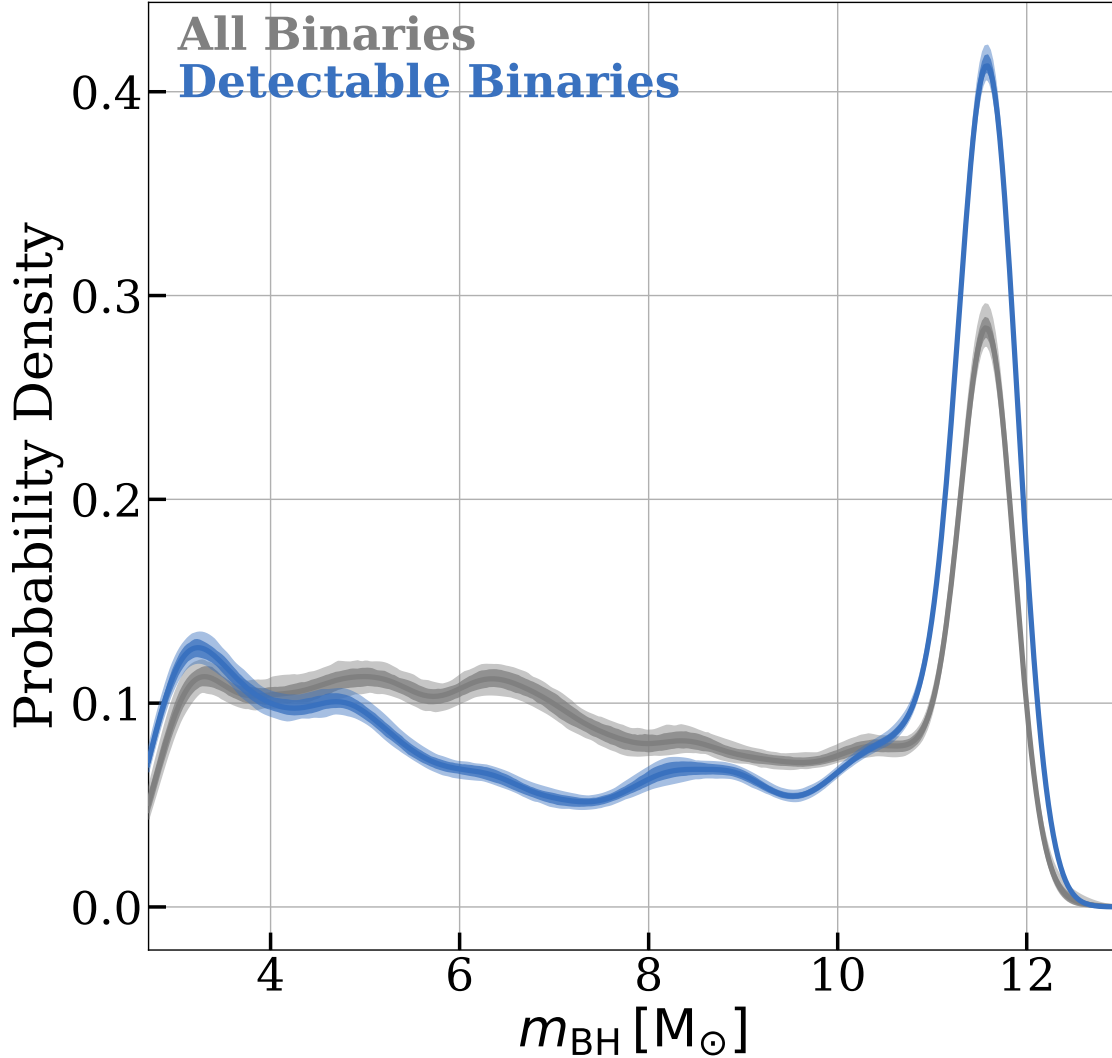
Figure A.1: A plot of the distribution of the black hole mass for both all binaries that merge in a Hubble time and all detectable binaries. The shape of the black hole mass distributions reflect the binary population results of COMPAS. There is a sharp cutoff at $M_{\mathrm{BH}} = 2.7 \, \mathrm{M_\odot}$, which is in agreement with the sharp cutoff in the birth distribution of masses, as discussed in section 3.1.1. Moreover, a majority of the black holes have masses greater than $10 \, \mathrm{M_\odot}$. The distributions between detectable binaries and all binaries are similar, with a slight bias towards greater black hole masses for the detectable binaries. This is because the strain is larger for greater masses (Eq. 2.18) and so systems with a larger black hole mass are more likely to be detectable.
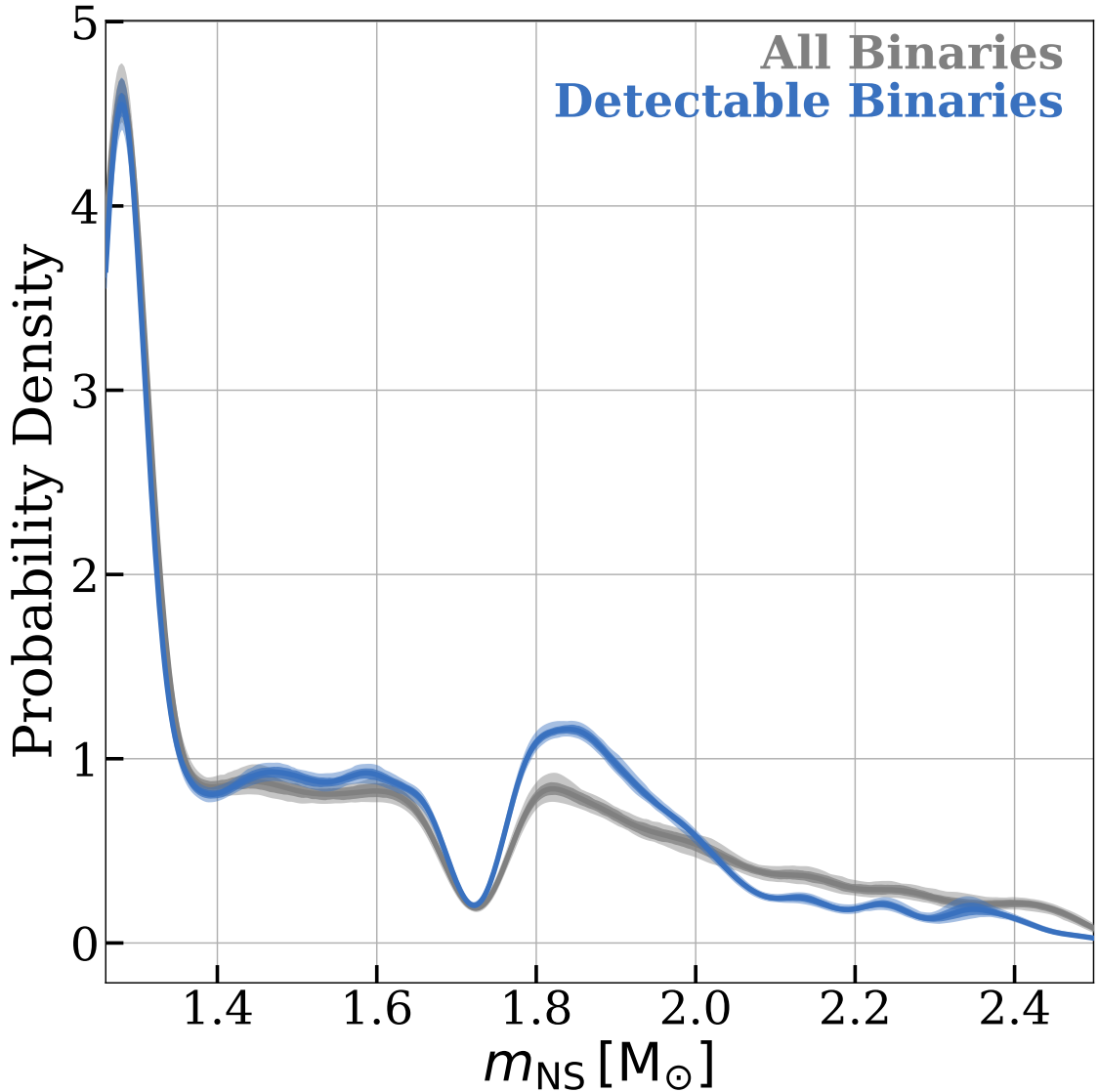
Figure A.2: A plot of the distribution of the neutron star mass for both all binaries that merge in a Hubble time and all detectable binaries. There is an excess of neutron star masses between 1.3 and $1.4\,M_\odot$. There is also a lack of neutron star masses are $1.7\,M_\odot$. This is a result of the discontinuity in the proto-compact object mass equation at carbon-oxygen cores of $M_{CO} = 3.5\,M_\odot$ (e.g. Fryer et al., 2012). This discontinuity is included in the COMPAS simulations and carries forward to affect the neutron star mass distribution. The two distributions are similar, with a slight bias towards greater neutron star masses for the detectable binaries. This is because the strain is larger for greater masses (Eq. 2.18) and so systems with a larger neutron star mass are more likely to be detectable. This trend is more evident for neutron star masses between 1.8 and $2\,M_\odot$ but not for the most massive binaries. The trend is likely not evident in the most massive binaries due to their scarcity in the sample, only 6% of binaries have a neutron star mass greater than $2\,M_\odot$.
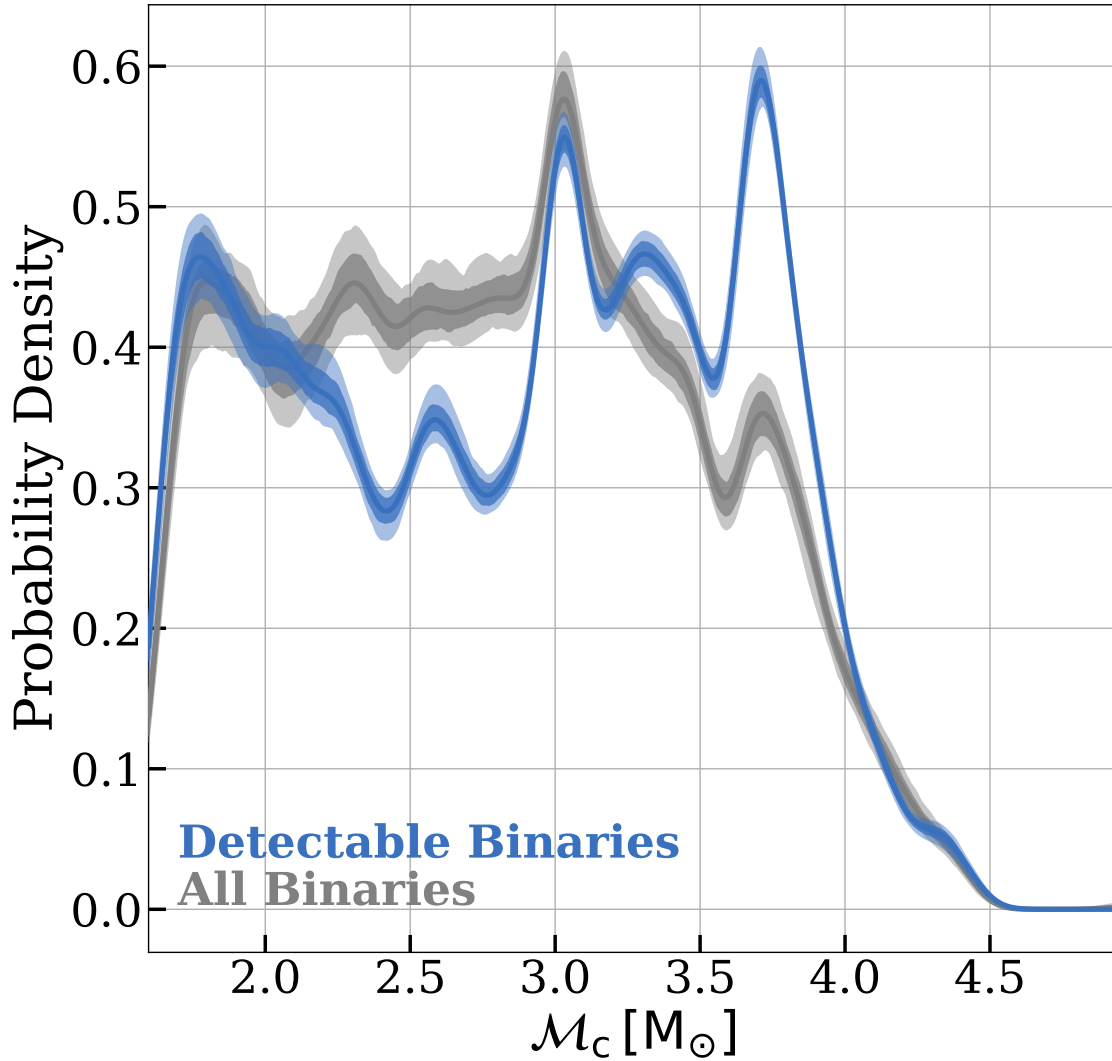
Figure A.3: A plot of the distribution of the chirp mass for both all binaries that merge in a Hubble time and all detectable binaries. Since the chirp mass is a combination of the two component masses (see Eq. 2.19), we see similar trends to the black hole and neutron star mass distributions (see Fig. A.1 and Fig. A.2). In particular, we note that the detectable binaries are skewed to higher masses.
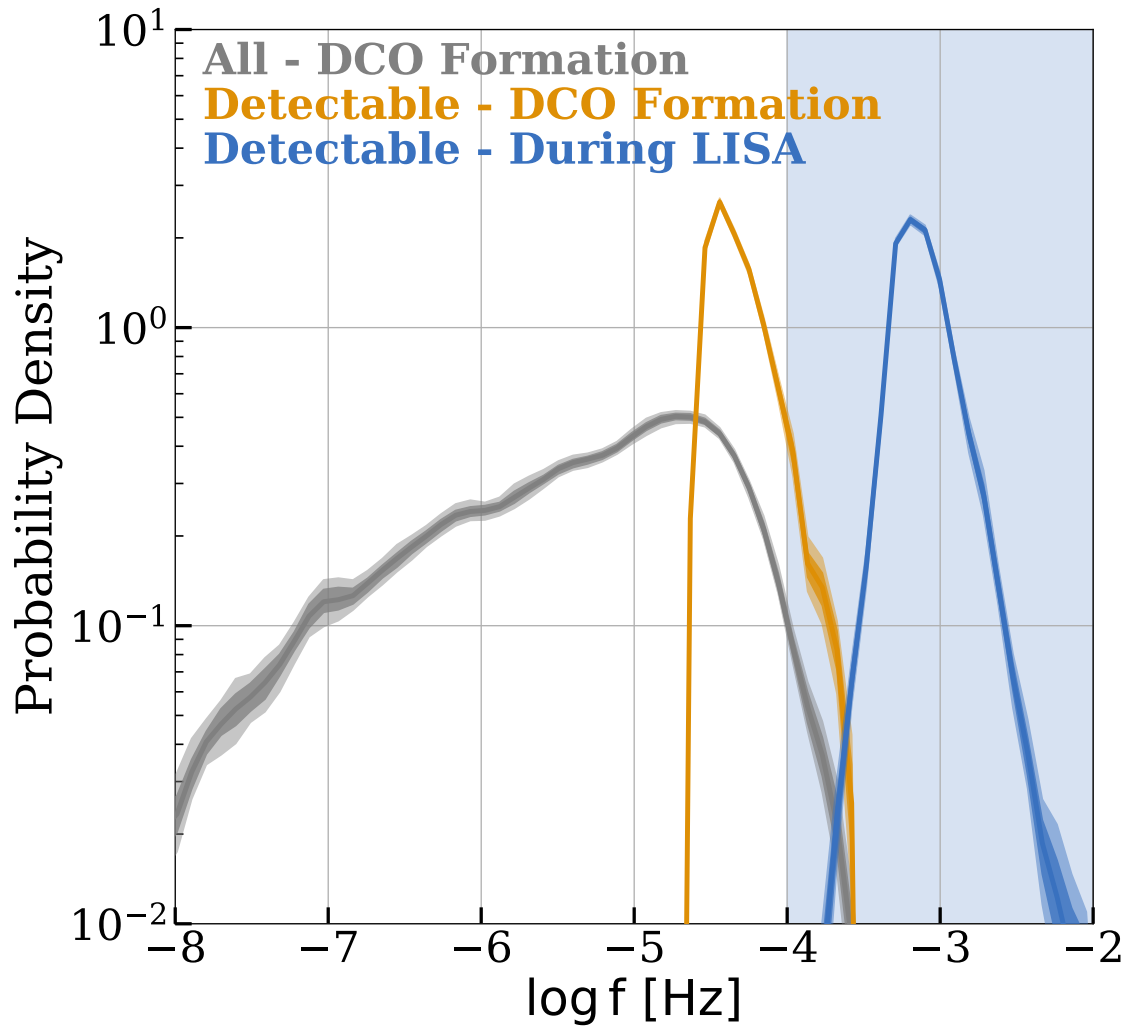
Figure A.4: A plot of the distribution of the gravitational-wave frequency for both all binaries that merge in a Hubble time and all detectable binaries, where the blue region indicates the LISA frequency band. This plots shows that higher frequencies are sharply favoured for detectable binaries. Given the LISA frequency band and that strain scales with frequency as $f_{GW}^{2/3}$, it makes sense that the detectable binaries are at higher frequency ranges.
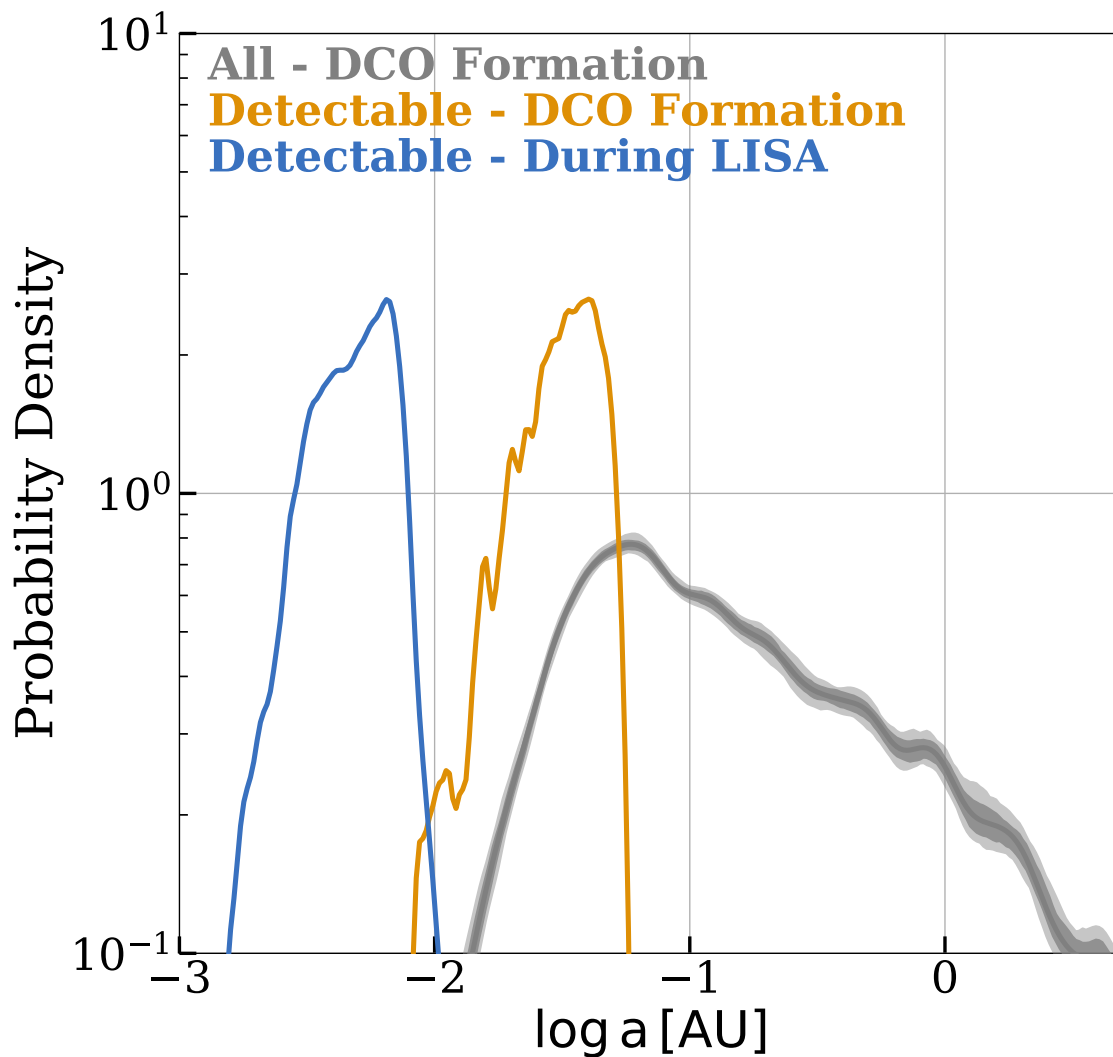
Figure A.5: A plot of the distribution of the binary separation for both all binaries that merge in a Hubble time and all detectable binaries. Smaller separations are sharply favoured. In particular, no detectable binaries are found with separations larger than 10^{-1} AU. Smaller separations are favoured by detectable binaries as the LISA frequency band corresponds to small separations and strain scales with separation as a^{-1} for circular orbits.
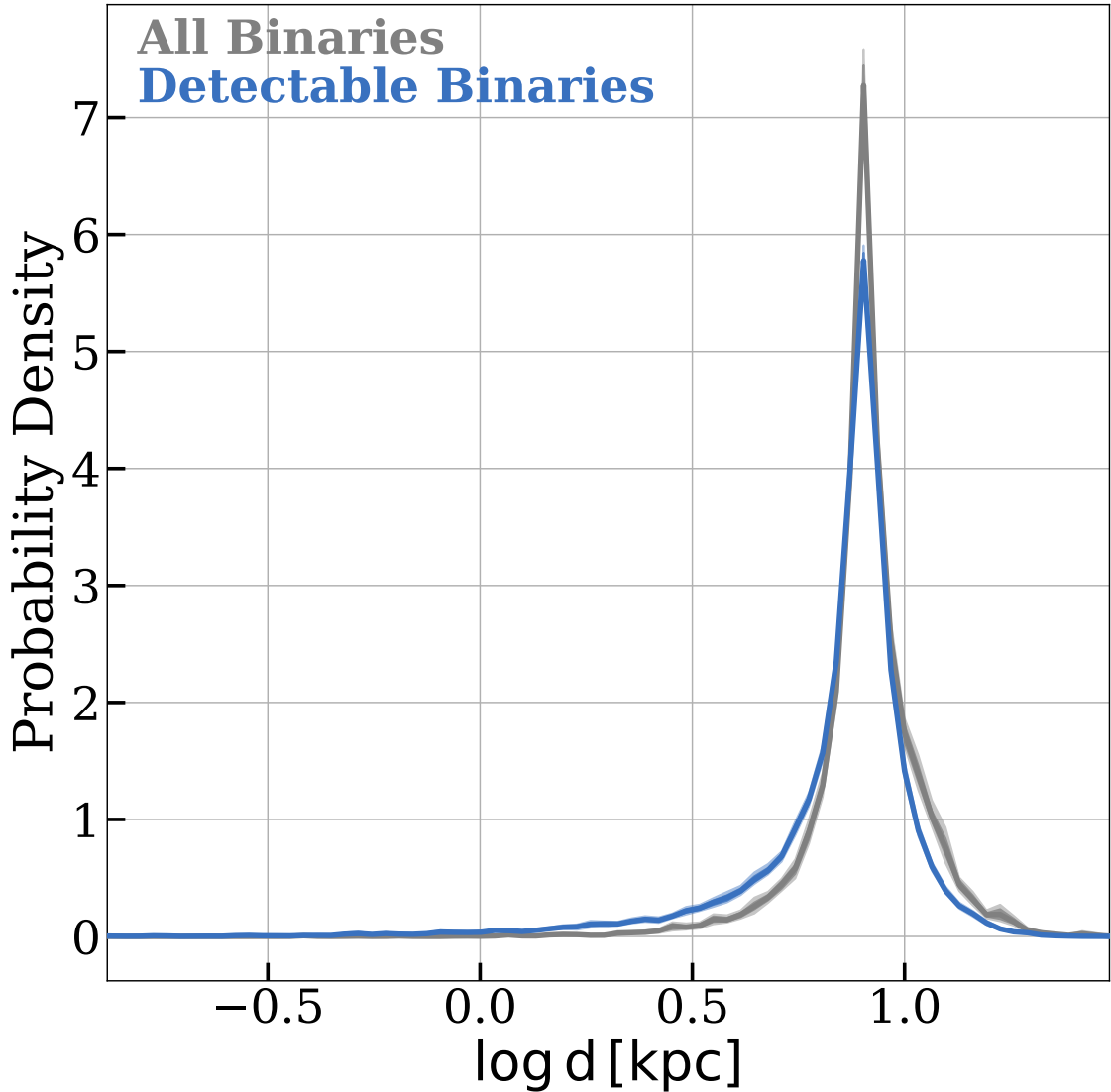
Figure A.6: A plot of the distribution of the distance to the gravitational-wave source for both all binaries that merge in a Hubble time and all detectable binaries. The distributions peak around 8 kpc and drops off rapidly for lower distances. Since we are using the density distribution for the galaxy given in section 3.2, most of the mass in the galaxy is concentrated around the centre. This explains the peak of the distribution 8 kpc, corresponding with our distance from the centre of the Milky Way. It is also notable that the distribution of detectable binaries is biased towards smaller distances. This is also expected, as we know from Eq. 2.18 that the strain is inversely proportional to distance. It is therefore easier to detect binaries that are closer.
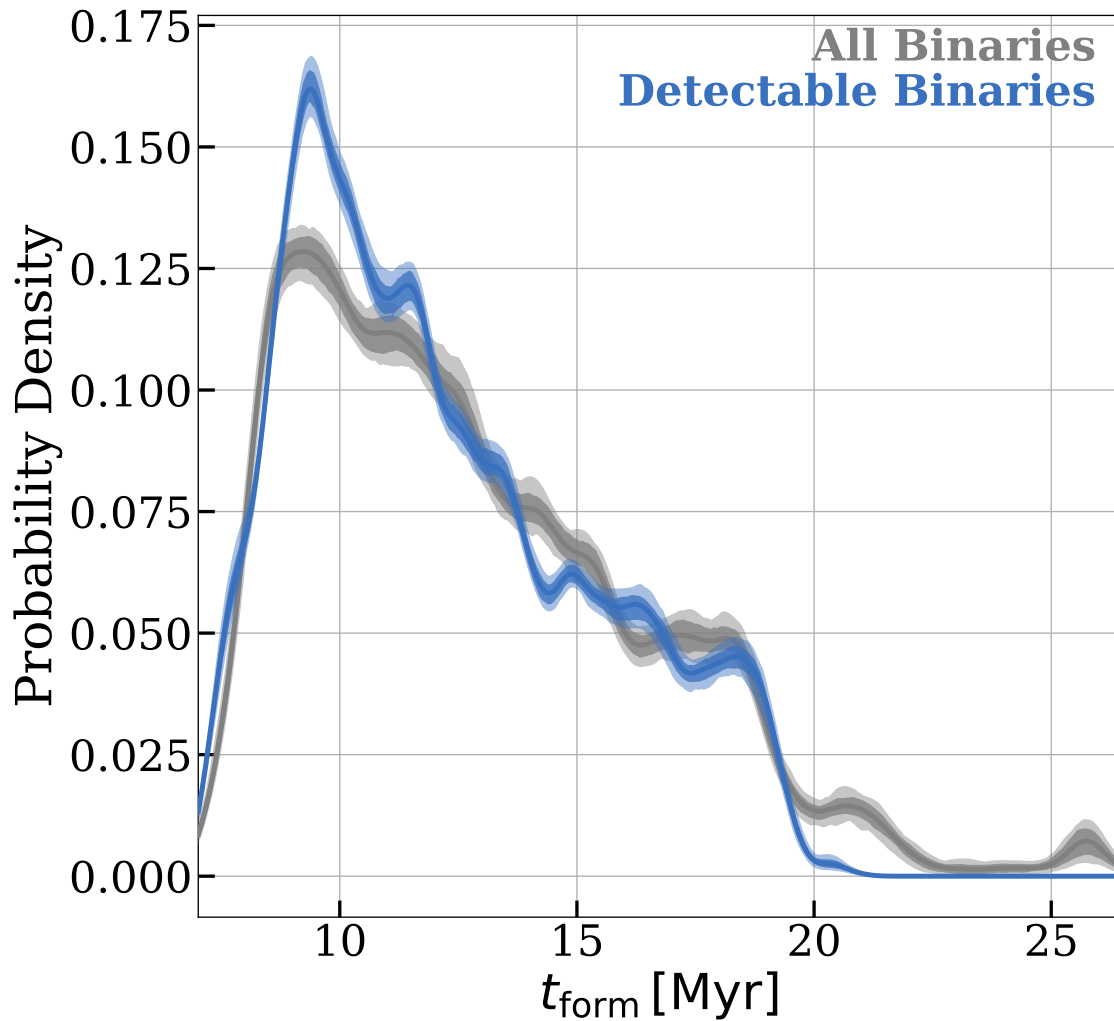
Figure A.7: A plot of the distribution of the formation time for both all binaries that merge in a Hubble time and all detectable binaries. The distributions peak around 10 Myr with a small spread, remaining within a factor of two of this peak. The distribution of all merging binaries and the distribution of detectable binaries are very similar, with only minor differences that can be attributed to statistical fluctuations.
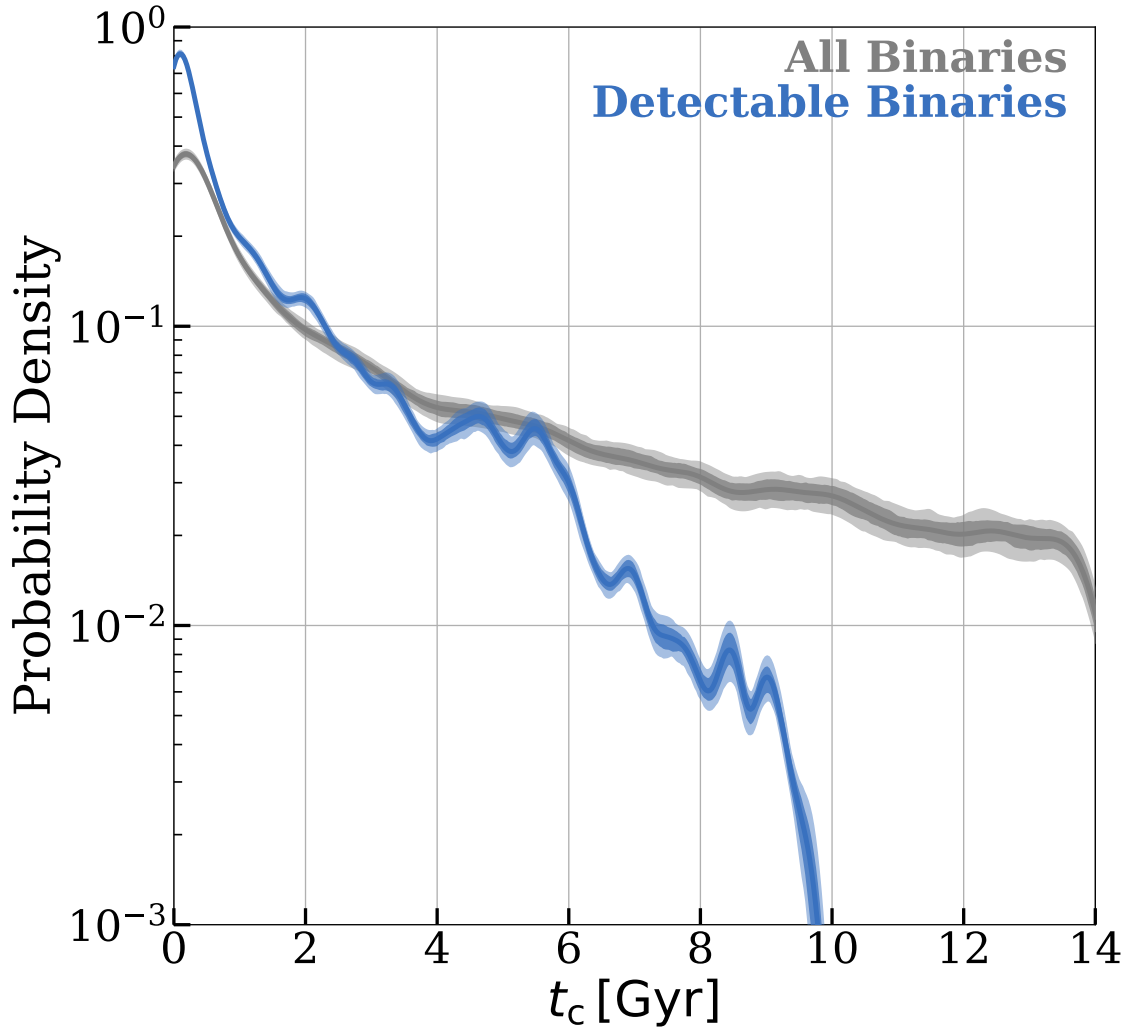
Figure A.8: A plot of the distribution of the coalescence time for both all binaries that merge in a Hubble time and all detectable binaries. The distribution for all merging binaries peaks strongly around 1 Gyr, with the majority of binaries coalescing in fewer than 2 Gyr. There is then a steep dropoff for larger times up a Hubble time. This upper limit is present because we imposed that all binaries must merge within a Hubble time in our initial assumptions. The distribution of detectable binaries is skewed towards shorter coalescence times. From Eq. 2.26, we know that the coalescence time scales at a^4 for circular orbits and the separations of detectable binaries are skewed towards smaller separations. Therefore, this explains the similar skew in coalescence times. There are no binaries detected with coalescence time greater than 10 Gyr, our age of the Milky Way, since any binaries with larger coalescence times would still have separations too great to be detectable by LISA.
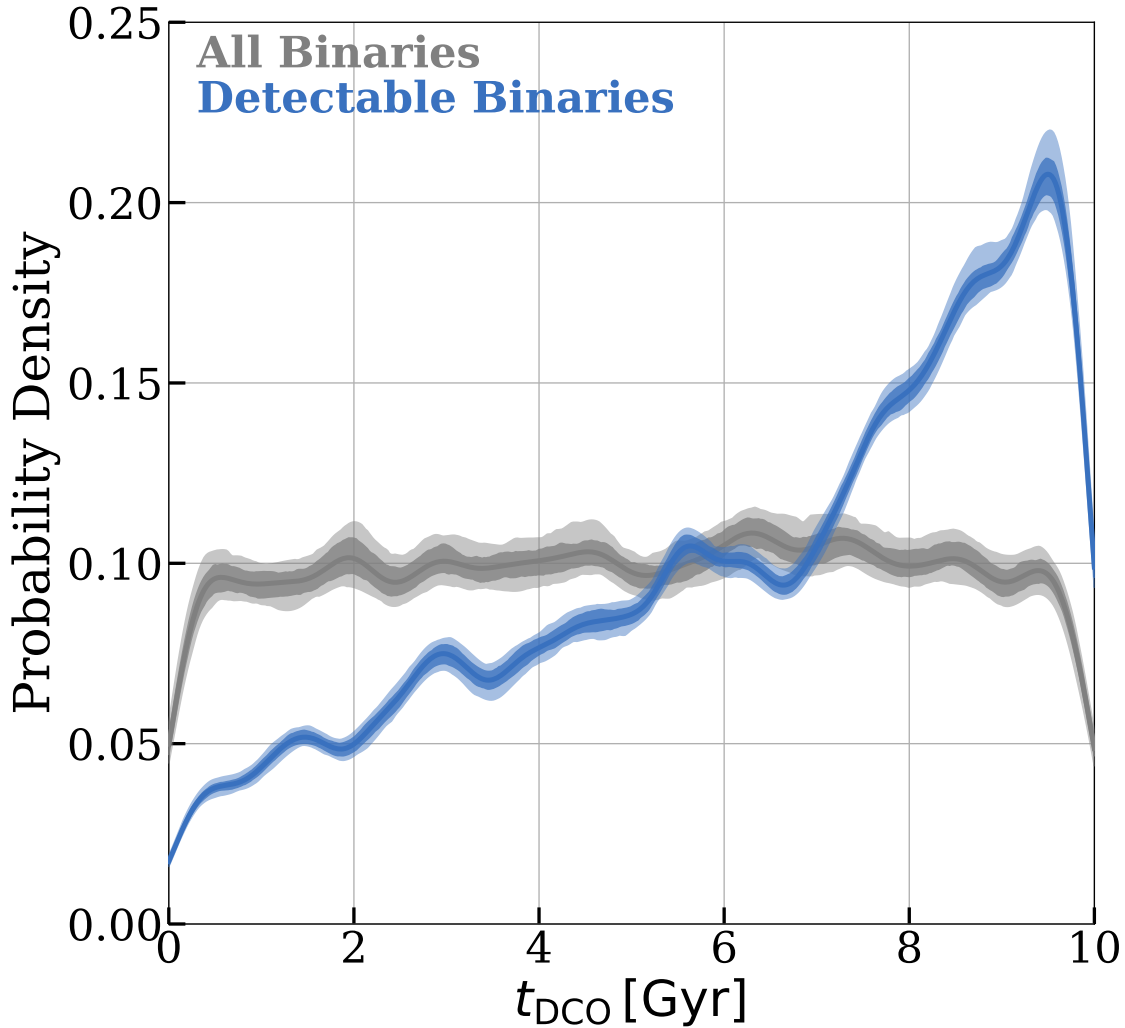
Figure A.9: A plot of the distribution of the DCO birth time for both all binaries that merge in a Hubble time and all detectable binaries. The distribution of all merging binaries is approximately uniform across the age of the Milky Way. However, the distribution of detectable binaries demonstrates a clear correlation between detectability and birth time. There are many more detectable binaries that were born recently than at the start of the galaxy. Upon comparison with the plot of coalescence time, this trend makes sense. We are most likely to detect binaries that have low separation since they produce the largest strains. However, the binary needs to not have merged before the LISA mission for us to detect it. The majority of binaries coalesce within 2 Gyr and therefore the binaries with the smallest separation during the LISA mission will have been formed 2 Gyr ago. Those BH–NS formed before will probably have already merged, and those BH–NS formed after the peak will have too wide separations to produce a strong enough strain. These expectations are shown exactly in the plot of the birth times.